UNIVERSITY OF TARTU
Faculty of Science and Technology
Institute of Physics
Information Technology

Henri Kuuste

ESTCUBE-1 TETHER END MASS IMAGING SYSTEM DESIGN AND ASSEMBLY

Bachelor's Thesis

Supervisors: M.Sc.E.E. Viljo Allik
M.Sc. Tõnis Eenmäe
M.Sc. Ilmar Ansko

Tartu 2012

Contents

Acronyms and abbreviations

ADC analog-to-digital converter

ADU analog-to-digital unit

CAN controller area network

CDHS Command and Data Handling System

CMOS complementary metal-oxide-semiconductor

COTS commercial off-the-shelf

DCMI digital camera interface

DMA direct memory access

EMC electromagnetic compatibility

EPS Electrical Power System

FIFO first in, first out

FITS Flexible Image Transport System

fps frames per second

FRAM ferroelectric random-access memory

FSMC flexible static memory controller

GPIO general purpose input/output

HDR high-dynamic range

HSE high-speed external oscillator

I^2C inter-integrated circuit

ICP Internal Communication Protocol

JPEG Joint Photographic Experts Group

LEO low-Earth orbit

MCO main clock output

MCU microcontroller unit

ND neutral density

PCB printed circuit board

RAM random-access memory

ROM read-only memory

RTC real-time clock

RTOS real-time operating system

SPI serial peripheral interface

SRAM static random-access memory

UART universal asynchronous receiver/transmitter

USART universal synchronous/asynchronous receiver/transmitter

USB universal serial bus

WDT watchdog timer

1 Introduction

The primary mission of the first Estonian student satellite, ESTCube-1 [1], is to test the electric solar wind sail principle in ionospheric plasma [2, 3]. In order to accomplish this, the CubeSat standard [4] based spacecraft will be launched into polar low-Earth orbit (LEO) and a small aluminium mass attached to the end of a 10 m long tether is to be reeled out using centrifugal force. The tether is then charged and the effect of ionospheric plasma on the angular velocity of the satellite is measured [3].

During this experiment, the deployment of the tether needs to be verified. Therefore, an imaging system capable of capturing the tether end mass at various distances from the satellite has been developed. On ESTCube-1 this system is also used to carry out the secondary objective of Earth imaging for outreach purposes [1]. Moreover, the camera has been designed as an independent module that is reusable in future spacecraft missions with extremely limited weight, volume, power, and communication bandwidth.

The goals of this work were stated as follows:

- List the requirements for the camera subsystem of ESTCube-1.
- Design an independent, robust, and reusable camera module for use in small satellites.
- Outline camera module firmware design.
- Create software for camera control and testing.
- Test the functionality and electrical characteristics of the resulting hardware.

The research presented in this study was conducted over a period of one and a half years. During this time preliminary studies were conducted, two hardware prototypes and the final engineering model were constructed and tested. Several iterations of firmware and detailed test plans were developed.

2 Overview of previous work

Previous research in small satellite camera systems has mainly focused on selecting suitable commercial off-the-shelf (COTS) camera modules or custom design of optics [5]. A general camera system design for pico- and nanosatellite application is proposed by K. Gulzar in his Master's thesis [6]. The system outlined in the research features an NXP Semiconductors LPC2468 microcontroller unit (MCU), Averlogic 512 kB first in, first out (FIFO) buffer, 16 MB random-access memory (RAM), 128 MB flash memory, and an OmniVision OV7720 imaging sensor with an external FIFO buffer. The resulting system has a power consumption of 1825 to 2825 mW and consists of two separate printed circuit boards (PCBs). Basic functional verification of the system was achieved; however, space worthiness has not been confirmed. [6]

Many small satellites with camera systems have been launched into space over the last decade. What follows, is an overview of some of the most notable of these small satellite cameras.

The Japanese satellites XI-IV and XI-V, launched in June 2003 [7] and October 2005 [8] respectively, use a 300,000 pixel 16 bit RGB complementary metal-oxide-semiconductor (CMOS) camera [9]. The system includes a FIFO memory for fast image transfer from the sensor, 224 kB read-only memory (ROM) and a PIC16LF877 running at 10 MHz for image evaluation and camera control [9]. After initial image capture, the images are resized to 128×120 pixels, allowing 7 images to be stored in ROM at the same time [10]. The image evaluation algorithm uses color, contrast and brightness to determine the usefulness of an image [10]. Both satellites successfully captured many images of Earth [11, 12]. Images from later stages of the missions show degradation in quality due to exposure to the space environment [13].

A larger Japanese satellite Cute-1.7 + APD II was launched in April 2008 [14]. This satellite contains a compact CMOS camera that was designed for use in mobile phones [15]. The camera is controlled by a Renesas' H8 microcontroller and its data is temporarily stored in a FIFO memory [15]. Connection to the on-board computer is achieved using the universal serial bus (USB) [15]. The camera is

used for attitude determination, Earth imaging and monitoring of tether deployment [16]. The satellite was able to capture at least 54 good quality images of Earth, from which both attitude and rotational speed were determined [15, 17].

The Tokyo University 8.5 kg nanosatellite PRISM, launched in January 2009 [18], is constructed as a telescope with a flexible boom [19]. For monitoring of the deployment of this boom, the satellite also includes 3 small wide angle cameras. These cameras were able to successfully take images of Earth and confirm the extension of the boom mechanism [20]. After the boom extension, images of Earth were overexposed due to the dark boom taking up large amounts of the image. However, Earth imaging was not the main mission of the small wide angle cameras. [21]

In June 2003 a Danish CubeSat, with a custom camera payload, called AAU CubeSat was launched [22]. The payload is based on a Kodak CMOS sensor providing a resolution of 1280×1024 pixels in 24 bit color [23]. The custom lens system is made of titanium and radiation hardened glass and provides a ground resolution of approximately 150×120 meters from a 900 km orbit [23, 24]. After launch, the satellite made contact with Earth; however, operations were severely limited due to problems with the on-board transmitter [24]. No images were received.

The Swiss satellite SwissCube uses a custom 50 mm telescope design for its airglow observation payload [25]. The camera is based on a highly sensitive Micron MT9V032 monochrome CMOS image sensor, Texas Instruments MSP430F1611 MCU, and 256×16 bit static random-access memory (SRAM) [26, 25]. Images are captured by using 4×4 pixel binning, giving an effective pixel size of 24 μ m and reducing the image storage requirements [26]. The satellite was launched in September 2009 [27] and many useful images have been captured [28].

A COTS OV7648 camera module was used on the German CubeSat Compass-1 [29]. The camera captures 8 bit VGA[1] format images and is controlled using the inter-integrated circuit (I^2C) bus [29]. The satellite was launched in April 2008 [30] and has received several images from the on-board camera. However, there were problems with the automatic exposure loop and the images are overexposed, despite the neutral density (ND) filter included in the system [31].

[1] Video Graphics Array

The Canadian Nanospace eXperiment (CanX) program has launched two satellites with similar camera systems. CanX-1 was launched in June 2003 and lost contact with Earth [32]. CanX-2 was launched in April 2008 and contact was made; however, no results have been published for the camera systems [33]. Both satellites have two independent COTS imagers manufactured by Agilent for CanX-1 and by National Semiconductor for CanX-2. A color imager is used for Earth imaging and a monochrome imager for star tracking. [34, 35]

The Turkish student satellite İTÜ pSat I also includes two separate camera payloads. The primary payload is a low resolution camera for continent-scale Earth imaging and the secondary payload is a low power CMOS imager, capable of taking JPEG pictures of Earth at a ground resolution of approximately 757×567 km. The imagers are controlled by a Texas Instruments MSP430F1611 MCU using the I^2C bus. The satellite was launched in September 2009 and a clear beacon has been received; however, no results have been published for the camera systems. [36, 37]

3 Imaging system requirements

3.1 General requirements

The main goal is to design a small, reusable and reliable camera module, which is able to function in the space environment without any external electronics. Due to the nature of a satellite mission, no changes can be made to the system once it is in use and contact with Earth is made in short communication sessions with limited bandwidth. System hardware changes are impossible after acceptance tests and firmware updates will be difficult to perform due to the communication limits.

The camera structure has to be small enough to fit in a single unit CubeSat without taking up more than 5% of the available space in the 1 liter cube. Interfacing the camera should be as simple as possible. Any failure in the camera system should not cause failures in other parts of the satellite. For reusability there should be several common interfacing options such as controller area network (CAN), universal asynchronous receiver/transmitter (UART), and serial peripheral interface (SPI).

Since the camera is partially exposed to the sun, it must function in a wide range of temperatures. Exposure to the space environment also means that the materials have to be chosen carefully. Outgassing, focus shift and deterioration of the quality of optical components and image sensor are the main concerns. Hence, most plastics and composites should be avoided, if not specifically designed for this kind of environment [38]. During launch the satellite will experience strong vibrations [39] and the camera has to be able to withstand this without loss of focus. Effects of radiation exposure should also be taken into account [40].

Based on the results from other satellites, it is clear that image redundancy would be required to increase the probability of acquiring a correctly exposed image. The camera should be able to take multiple images in quick succession to allow for exposure bracketing. It is known that radiation can cause random artifacts in the image sensor pixel array. Taking multiple images of the same object will enable the filtering of these artifacts in software. Manual control of camera settings is also recommended, in case there is an issue with any of the algorithms.

The independent camera module should include enough processing power to do all the image processing and compression needed. Image processing is needed for

automatic exposure determination and preparation for image transfer. The latter can include processing operations such as assessment of image quality, cropping, resizing and compression. Basic pattern detection and other more complicated image processing operations should be kept in mind for future applications. However, the module is designed as a supporting system rather than a primary payload, so power consumption should be kept to a minimum.

3.2 ESTCube-1 specific requirements

The ESTCube-1 tether end mass imaging module has to fit in the limited space available for it on the second payload PCB (see Figure 1). The position of the opening in the side panel is fixed. The camera structure has to be constructed in such a way that the optical axis is at the center of this opening. Table 1 lists the main requirements for the ESTCube-1 camera subsystem based on the initial budgets set for the satellite.

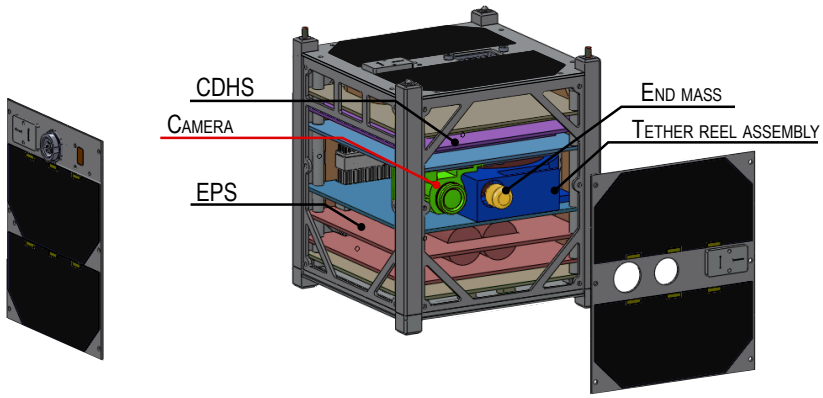

Figure 1. Positioning of camera and tether end mass inside ESTCube-1. [41]

On ESTCube-1 the camera is used to take images of Earth before the main mission and to monitor tether deployment at the early stages of the electric solar wind sail experiment. Therefore, the operating time frame of the camera is just a few months and long-term radiation effects are not of great concern. Using radiation shielding, radiation tolerant components, or hardware redundancy would increase

the size and mass of the whole system. Since the camera is not a critical system, size and mass are considered to be a priority over radiation tolerance.

Table 1. Primary requirements of the tether end mass imaging system. [42, 43]

Parameter	Value	Unit
Aperture	≤ 14	mm
Depth of field	$1.0 \ldots \infty$	m
Operating temperature range	-14...+59	°C
Supply voltage	2.8...5.5	V
Power consumption	< 350	mW
Dimensions (W $\times$ H $\times$ D)	$45 \times 25 \times 45$	mm
Mass	< 50	g

For single event effects it is assumed, that the Electrical Power System (EPS) of the satellite already includes single event latchup protection for the camera system. The software design of the camera should take into account the single event upsets that can cause bit flips in both data and code.

The most important performance requirement for the imaging system is the ability to produce images with good enough resolution to verify tether deployment. Thus, the tether end mass (illustrated in Figure 2) at a distance of 10 m has to be visible as at least a single bright pixel. The images for this can be monochrome and it can be approximated, that the reflected light from the end mass will be evenly distributed in all visible wavelengths.

The estimated brightness of an 40% sunlit end mass, when the tether is fully deployed, is about -7.3^m, which is much brighter than brightest planet – Venus in the sky [44]. The tether end mass can be considered stationary in the field of view of the camera, while the background is moving. The limiting factor for exposure is the rotation of the satellite, since tether end mass imaging should be done against a black background. At the start of tether deployment the satellite will be rotating at 1 revolution per second. At full tether extension, the angular velocity is assumed to go down to 1 revolution per 30 seconds. As a result of the low-Earth orbit, it can be assumed that Earth will be in direct line of sight for about half of this time.

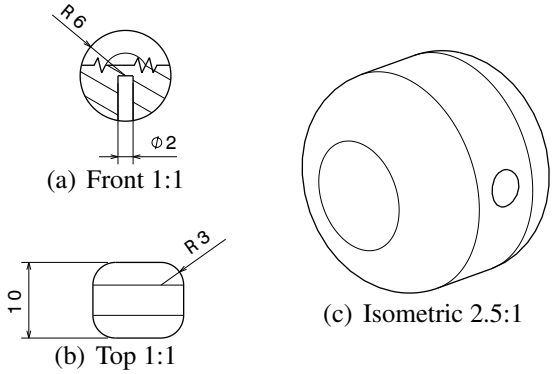

(a) Front 1:1

(b) Top 1:1

(c) Isometric 2.5:1

Figure 2. Mechanical drawing of the tether end mass. [41]

Secondary requirements arise from the ability to take color images of Earth for educational and public outreach purposes. It is desirable to have Estonia recognizable in the images, if the satellite is able to capture images of the region with minimal cloud cover. Exposure times for Earth imaging should be very short, to avoid overexposing the image and minimize the smearing caused by the motion of the satellite. The camera parameters for Earth imaging are similar to photographing sunlit ground and clouds from Earth.

Additional constraints are set on the camera based on the estimated downlink transfer rate of 9600 bps. The imaging system should do as much as possible to reduce transfer size for each image, while maintaining the required image quality.

4 Camera design

4.1 Hardware

4.1.1 Overview

Many commercially available camera modules and design solutions were considered. The modules specifically designed for the CubeSat standard, such as the STAR-1000 [45], do not meet most of the requirements set for ESTCube-1. End mass imaging quality requirements make the use of lossy compression impossible. This, combined with field of view, material and size requirements, rules out most COTS camera modules. The existing camera systems do not in general include memory and processing power to manage multiple images, hence an external MCU and memory module would be needed. Taking all of this into consideration, no suitable COTS module was found. It was decided, that a complete camera electronics system would have to be designed from basic components. Standard optics would be used, since development of custom optics would take too much time and limit the use of the system in future applications. Figure 3 shows the hardware design of this system.

In the hardware design and layout electromagnetic compatibility (EMC) principles were observed. Recommendations from Nokia [46], Texas Instruments [47] and STMicroelectronics [48] were used in creating a robust camera module.

Based on these recommendations most of the unused pins have been connected to electrical ground, in order to avoid an accumulation of charge on floating pins. Filters for high frequency noise have been added on external connections. Where possible, high frequency signals have been isolated from noise critical signals by using strips of ground plane. To ensure low resistance, through-hole vias are densely distributed on the ground planes.

Initial prototypes (see Figure 4) used a 4 layer PCB design, since this was easier to create and size restrictions were not an issue in prototyping. The final design (see Figure 5), however, has to use 6 layers to minimize the camera system size and noise in high frequency signals. Component size is also an issue, with the MCU being the largest. However, for reliability, ball grid array (BGA) and similar

packaging is to be avoided. Where possible, larger and less dense components are used, to minimize the effects of radiation.

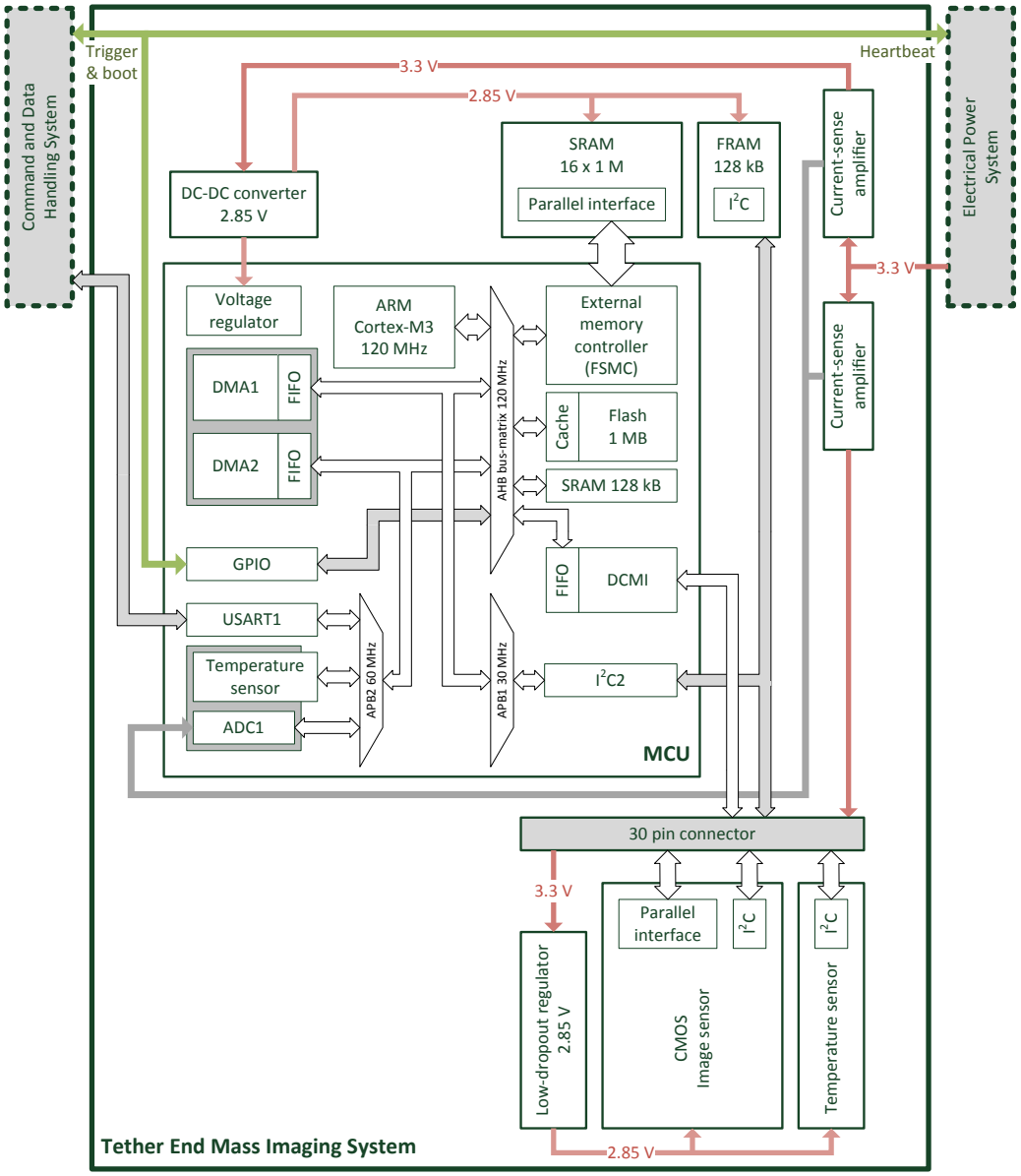

Figure 3. Hardware design block diagram for the ESTCube-1 camera module. The major blocks in the diagram are explained in the hardware design of this paper and the acronyms are expanded in the Acronyms and abbreviations section.

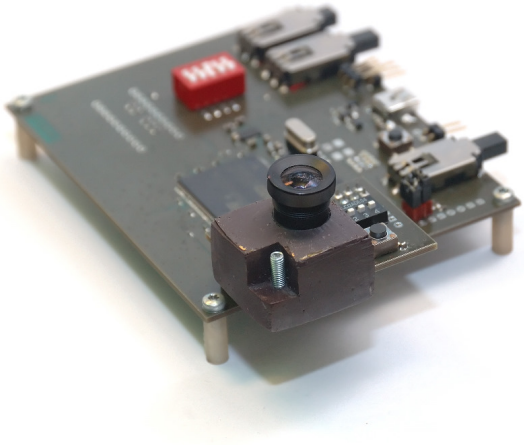

Figure 4. Photo of the second camera prototype.

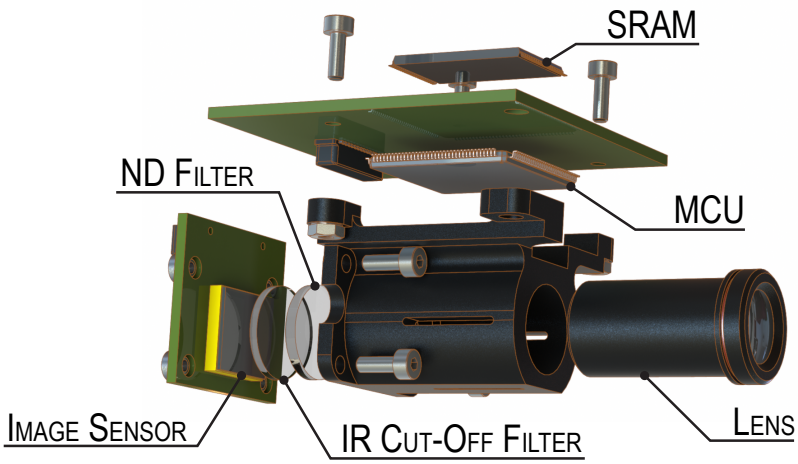

Figure 5. An exploded view of the final camera module design, where SRAM stands for static random-access memory, ND for neutral density, MCU for microcontroller unit, and IR for infrared.

4.1.2 Sensor

The image sensor MT9V011 from Aptina was chosen mainly due to availability and the parameters listed in Table 2. Of particular concern were the image resolution, pixel size, and temperature range.

Since the image sensor has an electronic rolling shutter, the pixel integration time depends on the rate at which data is transferred out of the image sensor. This

places additional speed requirements on both the microcontroller and the memory. The use of an intermediate FIFO memory would reduce these constraints; however, it would increase complexity and possibly power consumption.

Table 2. Main parameters of the MT9V011 image sensor. [49]

Parameter	Value	Unit
Diagonal	$\frac{1}{4}$	inch
Active pixels (H $\times$ V)	640×480	
Pixel size	5.6×5.6	μ m
Color filter array	RGB Bayer pattern	
Operating temperature	-20...+60	°C
Bits per pixel	10	
Frame rate	30	frames per second (fps)
Power consumption	< 70	mW

The sensor PCB is at a right angle to the main board that holds the rest of the electronics. Initially flexible cable and printed circuit connectors were considered. However, due to availability, cost and structural issues, a rigid right angle connector with 30 pins at a pitch of 0.8 mm is used in the final design. The length of tracks carrying high frequency signals on both the PCBs is kept to a minimum and the corresponding connector pins are surrounded by ground to minimize noise. The separate image sensor PCB also allows for easier replacement of the sensor for future missions and different applications.

The lens mount, designed by Ants Agu (see Figure 5), uses a standard M12 $\times$ 0.5 thread. This results in a more flexible system allowing for easy replacement of the lens. For the ESTCube-1 mission the Edmund Optics NT57-908 lens is used. This is a 4.4 mm telecentric lens with a focal ratio of 1.85. Giving the camera a field of view of 46 $\times$ 35 degrees and a resolution of 262 arcseconds per pixel. For tether end mass imaging at a distance of 10 m this translates to 12.7 mm per pixel. For Earth imaging at a height of 600 to 800 km this corresponds to 0.76 to 1 km per pixel.

Given the field of view of 46 degrees in the spin direction, Earth will be visible in the image for 63% of the time, or 630 ms at the start of tether deployment. This

means that 370 ms are available for tether end mass imaging against a dark sky background. At the sensor full speed of 30 fps, 11 images can be captured during this time.

4.1.3 Microcontroller

At the start of the tether end mass imaging system design process, a microcontroller had already been chosen for the Command and Data Handling System (CDHS) [40]. Since software development and testing are major issues in the design of embedded systems, the camera module uses a processor from the same family. This enables the sharing of code and reduces the amount of testing.

Due to the necessary memory and camera interfaces, initial prototypes were made with the STMicroelectronics STM32F103ZE, a 144 pin version of the processor that is used by CDHS. The second version of this prototype is illustrated in Figure 4. The sensor was interfaced using general purpose input/output (GPIO) ports and direct memory access (DMA). The built in DMA controller of the processor, however, proved to be a bottleneck, limiting image transfer speed to only a quarter of the maximum 30 fps. Also the pixel clock synchronization for GPIO DMA transfers required external logic gates to create a trigger signal for the DMA controller.

During our prototyping phase, STMicroelectronics released a new generation of microcontrollers that had higher processing speed and a dedicated camera sensor interface. The final camera design was adapted to use the STM32F217ZG microcontroller. Table 3 lists the main parameters of this MCU.

Maximum power consumption is given for a situation where all peripherals are enabled. In the camera module this is unlikely to be reached since most of the peripherals are turned off. Estimated power consumption with all the required peripherals is about 120 mW.

To connect to the imaging sensor, the STM32F217ZGT features a digital camera interface (DCMI) capable of communicating with up to 14 parallel data lines. The DCMI features transfer rates up to 48 $\frac{MB}{s}$ and automatic image cropping functionality.

The sensor parameters are controlled using an I^2C bus. The same I^2C bus is also connected to an external ferroelectric random-access memory (FRAM) and an external temperature sensor. The FRAM is used for storing system configuration parameters and possibly some telemetry data.

Table 3. Main parameters of the STM32F217ZG microcontroller. [50]

Parameter	Value	Unit
Architecture	Cortex-M3	
Flash memory	1	MB
SRAM	132	kB
Operating temperature	-40...85	°C
Supply voltage	1.8...3.6	V
Operating frequency	120	MHz
Power consumption	< 176	mW

Image sensor clock is provided by a special main clock output (MCO) pin on the MCU. The microcontroller provides two of these pins, with some differences in which input clocks can be used [51]. Both provide a selection of 4 clock sources, which can then be divided by a prescaler for output onto the pin. For the current camera design the first MCO pin is used with the high-speed external oscillator (HSE) as the source and a prescaler of 1. The 26 MHz crystal used to clock the MCU is very close to the maximum operating frequency of 27 MHz for the sensor. Initial prototypes using this design had serious issues with sensor clock stability and noise. However, these issues were resolved by making the main clock tracks as short as possible on the PCB, adding an additional 50 Ω resistor to the clock line and shielding the clock from other high frequency tracks.

The microcontroller also has a flexible static memory controller (FSMC) which allows for easy connection of the 16 bit external SRAM. The memory controller is able to operate at up to 60 MHz and features a built in FIFO buffer [50].

In the schematic and layout design for the processor circuit, recommendations from STMicroelectronics were observed concerning the lowest power consumption [52] and best reliability [53].

4.1.4 Memory

The camera needs to be able to store multiple images in quick succession. This means that an external memory module is required. Multiple different options were considered. Serial memory modules are small and easy to use; however, the speed of these devices would mean that the data from the sensor would have to be buffered somewhere while it is being written to the main memory. Since the built in MCU memory is not large enough to hold a full image, external buffers would be required.

For speed and simplicity it was decided to use a parallel memory module. Initial prototypes were built with the CY62167DV30 memory module by Cypress. This is an ultra low power memory with an access time of 70 ns. However, during testing and further development it became evident that faster transfer rates would be required for reliable Earth imaging.

As a result of this the Cypress memory was swapped for an Integrated Silicon Solution, Inc. IS61WV102416BLL-10TLI memory module. This is a high performance and low power CMOS 16 bit parallel SRAM. The main parameters listed in Table 4 are very similar to the module used during prototyping; however, it is much faster and uses more power.

Table 4. Main parameters of the IS61WV102416BLL-10TLI SRAM memory module. [54]

Parameter	Value	Unit
Capacity	16	Mbit
Word size	16	bit
Operating temperature	-40...85	°C
Supply voltage	2.4...3.6	V
Access time	> 10	ns
Power consumption	< 150	mW
Standby power consumption	< 75	mW

Power consumption is given for an access time of 20 ns. For image storage, at maximum pixel transfer rates from the camera, an access time of around 40 ns is

required. Resulting in further reduced active power consumption.

4.1.5 Housekeeping data sensors

Housekeeping data includes information about system operational status and is recorded for the purposes of satellite health monitoring. In order to collect this data, the tether end mass imaging system includes two separate current measurement circuits and two temperature sensors.

There are separate current measurement circuits for the image sensor PCB and the main PCB, allowing for more detailed analysis of power consumption. A temperature sensor with an accuracy of ± 0.5 °C is located behind the image sensor. The relative changes in image sensor temperature can be used to compensate for dark current and hot pixels in the image. A second, less accurate temperature sensor is located inside the MCU.

4.1.6 Schematics and layout

The schematics for the final design are given in appendices C and D. The corresponding PCB layout is shown in appendices E and F. This design includes wingboards for debugging. On the satellite these extra boards are removed and the main camera PCB is merged with the second payload board.

The debugging system includes various switches and light-emitting diodes for system control, pin header outputs for the satellite stack connections and SPI. Computer connectivity is achieved using two USB ports. One of these is directly connected to the full speed USB interface of the MCU and the other one is connected to the first universal synchronous/asynchronous receiver/transmitter (USART) channel using an RS-232 to USB interface.

4.2 Software

4.2.1 Overview

The camera control firmware consists of multiple interacting parts. A general overview of these is illustrated in Figure 6. Functionally the firmware can be divided into the following parts:

- background tasks such as
  - heartbeat,
  - housekeeping data collection and
  - time synchronization;
- image capture and storage;
- image processing;
- communication and command processing;
- camera configuration management;
- firmware update management.

Many of the tasks of the camera control firmware have to be run at specific times or even simultaneously. To facilitate this, a real-time operating system (RTOS) is used. For the purposes of sharing code, the camera subsystem uses the same FreeRTOS kernel as CDHS. All low level drivers and general interfaces are shared between subsystems.

Software errors in the system can arise from multiple factors. The most important of these are radiation and other external interference sources. The main effects of these interferences to software are:

- code corruption,
- data corruption,
- and unscheduled resets.

Code and data corruption can be either permanent (hard errors) or temporary (soft and firm errors). In order to deal with permanent code corruption, the only option available to the camera system, is to upload the new firmware to the microcontroller. For this purpose firmware images for all subsystems are stored on CDHS

and EPS. The camera subsystem contains two bootloaders for redundancy. Temporary code corruption is dealt with by the use of both a watchdog timer (WDT) and a heartbeat signal generator.

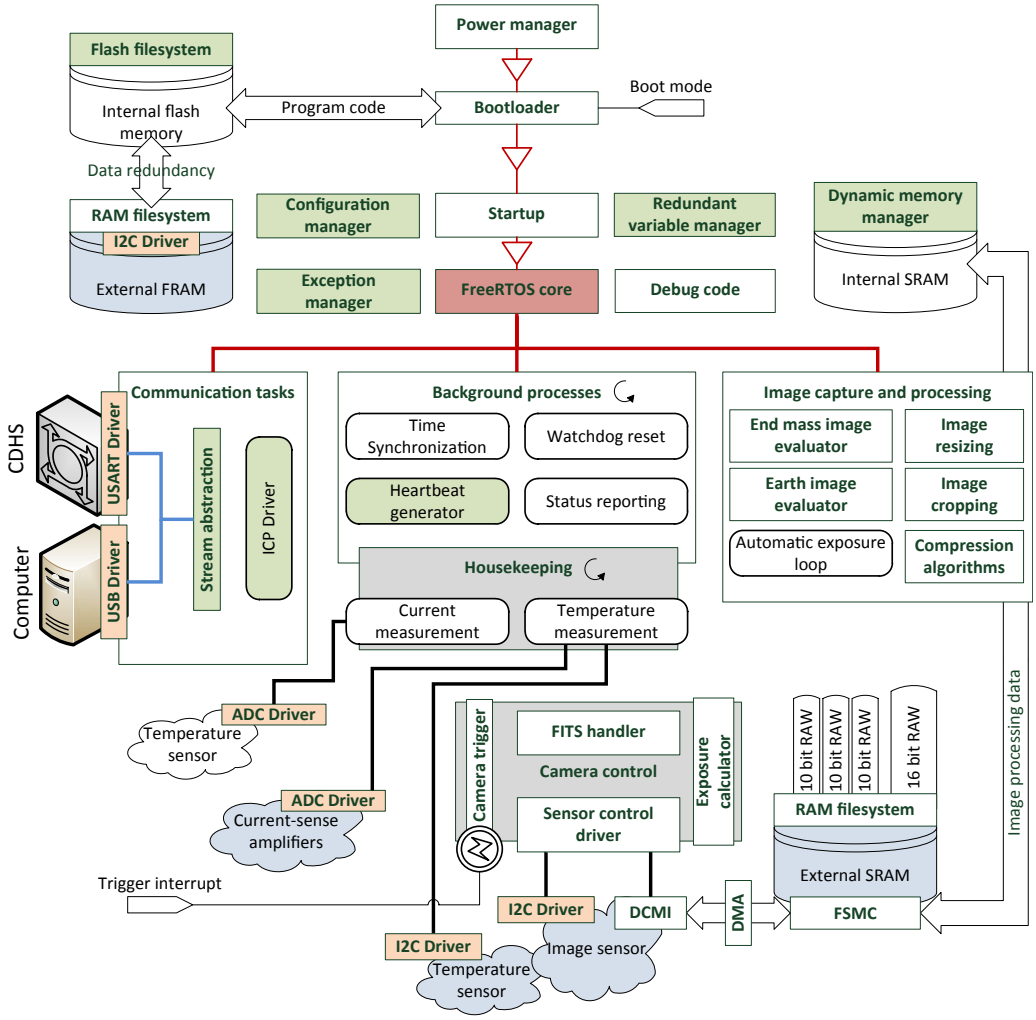

Figure 6. An overview of the camera firmware design. The green and orange colors represent major blocks of shared code. Green for high level code and orange for low level STM32 specific code. Acronyms are explained in the Acronyms and abbreviations section of this paper.

For dealing with data corruption the system includes several redundancy systems. Firstly all of the critical data has 3 copies in memory. This also applies to temporary variables used in code. Special macros are used to work with these variables

and data segments. Secondly multiple copies of critical permanent data is stored in both the flash memory of the microcontroller and an external FRAM module. When reading any of the redundant data a voting system is used to determine a value to return. Configuration data is also checked against a checksum at system startup. Configuration backups can be requested from external systems when all internal backups have failed. Images are not considered critical data, since new images can be acquired. Moreover, corruption of parts of an image does not affect the rest of the image.

4.2.2 External interfaces

The Electrical Power System (EPS) provides power (3.3 V and a maximum of 200 mA) and an additional level of error checking to every subsystem. To facilitate this, a heartbeat signal is generated by the subsystem. EPS monitors this signal and can decide to reset or power down the subsystem based on this information.

While in imaging mode, the camera module waits for a trigger interrupt. Using a general purpose interrupt line, CDHS can use its own scheduling and timing logic to trigger the camera at a precise moment in time.

When the camera is running, it can use the USART interface to send and receive commands to and from CDHS and the rest of the satellite using the Internal Communication Protocol (ICP). This is used to set up camera parameters and send images to CDHS for storage. Telemetry data is sent to CDHS at regular intervals. When in bootloader mode, the same USART interface can be used to upload new firmware to the camera. A custom bootloader allows for precise changes to the firmware without resetting any of the settings stored in microcontroller flash memory. As a backup option, the trigger control line can be held high during camera startup. The system will then enter a factory programmed bootloader and allow all of the flash memory to be overwritten. Camera configuration presets can be stored in flash and FRAM. A set of reasonable presets is included before launch.

CDHS contains a real-time clock (RTC), the camera can synchronize with this at regular intervals in order to obtain correct timestamps for image capture. The timestamps stored in image headers, can later be used to determine the location of the satellite during Earth imaging.

4.2.3 Image sensor interface

The camera control processor has full control over the image sensor. Firstly it controls the voltage regulator and can completely cut power to the sensor. Secondly it is connected to all the control lines of the sensor, allowing it to set the sensor in a standby mode and control when the sensor is actively integrating pixels and outputting data. I^2C is used to set up and control the operation of the image sensor.

The 10 bit data bus and synchronization lines are connected to the digital camera interface of the microcontroller. Fast DMA is used to transfer images to the external SRAM module. This memory is connected to the microcontroller using the FSMC interface and is set up for 16 bit data transfers. As a result every image is initially stored as 16 bits per pixel, where the upper 6 bits are 0.

Initial prototypes of the camera system did not have the DCMI interface. A custom camera interface was created using general purpose input/output, interrupts and DMA. However, the speed of the general DMA channel was a limiting factor in this application.

4.2.4 Housekeeping data collection

An analog-to-digital converter (ADC) is configured to take continuous readings using DMA. The readings are stored in a circular buffer in RAM. The ADC uses 4 channels to measure internal voltage reference, internal temperature, and two current-sense lines. Image sensor temperature is obtained using I^2C. Errors and resets are logged in internal RAM and backed up in external FRAM. The collected data is accessed in a status reporting task, that sends this data to the external interfaces.

4.2.5 Image capture and processing

All images are transferred to a special 614.4 kB memory region in the SRAM, which is able to hold a full image at 16 bits per pixel. After transfer the 16 bit image data is packed into a 10 bit format and stored in separate regions in the memory. The size of such a packed image is 384 kB. Using this layout, a total of

4 images can be stored in the 2 MB memory module. The remaining 233.6 kB is used for thumbnails, cropped images, compression and any other image processing needs.

All images are stored in the Flexible Image Transport System (FITS) format and include the following header information:

- exposure,
- gain for all four pixel types in the Bayer pattern,
- time of capture (this is obtained from CDHS),
- image sensor temperature,
- firmware version,
- and a comment with camera mode and other configuration parameters.

Additional header fields are used during testing to store parameters relevant to the specific test such as the measured brightness of a test light source.

The image capture process depends on the type of image expected. All images are compressed before transfer to Earth. The exact compression algorithm has not yet been selected, since it requires further testing. The main candidates are run-length encoding with bit planes and the Lempel–Ziv–Markov chain algorithm. Including a lossy compression algorithm option, such as JPEG, might also be considered for preview images of Earth.

4.2.5.1 Tether end mass imaging

During tether end mass imaging, the camera is attempting to detect a small bright object, which, at full tether extension, will appear as a single pixel. However, both radiation and temperature artifacts also result in small bright spots in the image. Therefore, the capture process, outlined in the following steps, focuses on the filtering of artifacts and the selection of likely image areas for tether end mass capture.

1. Four images are captured with a configurable interval and manual exposure settings.

2. The images are filtered and combined to remove random hot pixels and other temporary artifacts in the images.
3. The position, size and brightness of bright spots in the resulting image are listed. The threshold for detecting these areas in the image can be configured externally. Each such bright spot may be the end mass.
4. The image and the list of bright areas is stored in CDHS. If no bright areas matching the criterion were found, this is also reported.
5. The list of bright spots is sent to the ground station, where it is decided which of these locations are of interest. A list of requested image areas is sent to the satellite.
6. The image is transferred back to the camera subsystem from CDHS memory.
7. The requested image areas are cropped, compressed with a lossless algorithm and sent back to CDHS for transfer to Earth.

4.2.5.2 Earth imaging

Due to the increased visual complexity and resulting compressed image size, the Earth imaging process is more complicated and is summarized in the following steps.

1. A capture mode is set by CDHS using the following configuration options.
    - Single image or multiple images with specific capture interval.
    - Automatic exposure or manual exposure. In automatic exposure mode, multiple images are taken in a loop prior to actual capture. A histogram is formed for each such early image and exposure is calculated based on the amount of visible information in the center of the histogram.
    - Exposure bracketing. In this mode the calculated or preset exposure is modified by a configured multiplier to get a set of images of the same object at different exposures.
2. The images are captured when a trigger interrupt is received.

3. An image evaluation algorithm is run on each of the images. This algorithm is similar to the one used by the Japanese XI satellites [10]. The system calculates a weighted sum of factors such as brightness, contrast, hue, saturation and histogram balance. Each of these factors are also stored separately for reference.
4. Small compressed thumbnails are generated for each image.
5. CDHS sends image evaluation results to the ground station.
6. A ground station operator can then request thumbnails for additional evaluation of images. Any part of the full images can then be requested, specifying crop, resize, and compression options. It is also possible to request a combined 16 bit high-dynamic range (HDR) image from any of the captured images.
7. Images are sent back to the camera system, where the specified operations are applied to the images.
   When a HDR image was requested, the specified images are combined in a floating point format based on exposure and gain values in the FITS headers. The resulting image is converted to a 16 bit integer format based on the minimum and maximum HDR values.
8. The results are sent to Earth.

5 Testing

5.1 Testing software

For testing purposes camera control application called PyCAM was written in the Python programming language. The overall structure of the application is shown in Figure 7. The user interface for the application (see Figure 8) was written using PyQt.

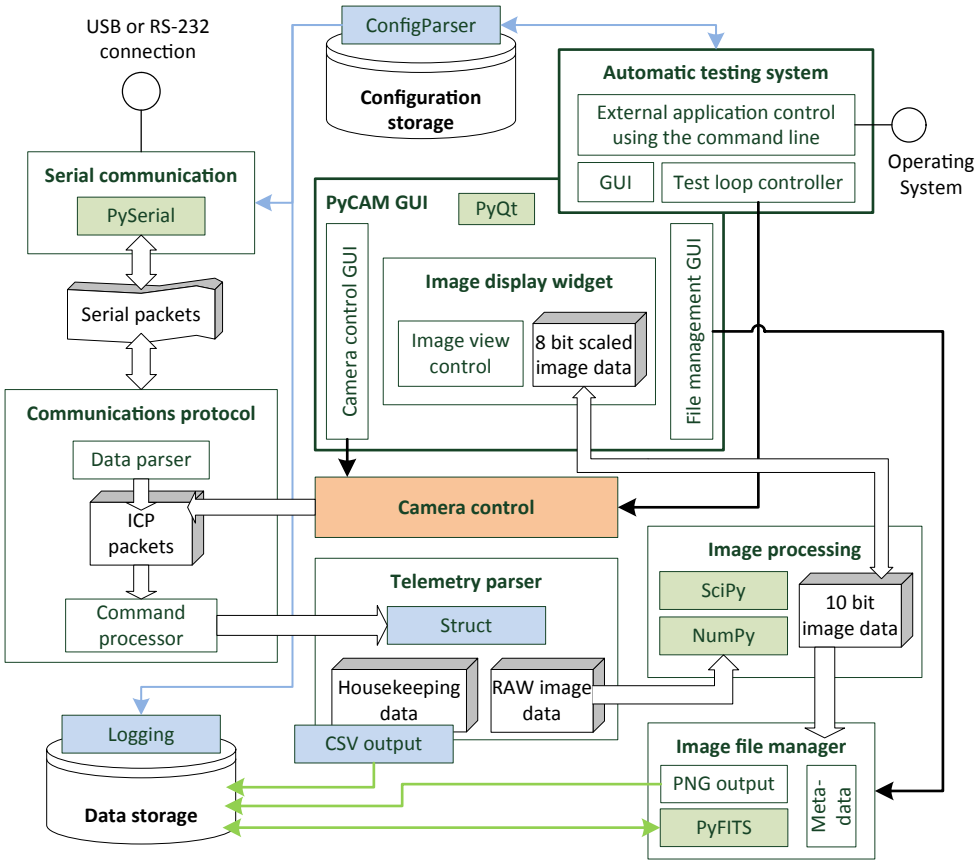

Figure 7. An overview of the PyCAM camera control software.

The application implements a basic version of the ICP used in the satellite. The camera is connected to the computer using either RS-232 or USB. The debug version of camera firmware includes a USB peripheral driver that appears to the computer as an RS-232 port. PyCAM connects to the serial port and uses ICP to

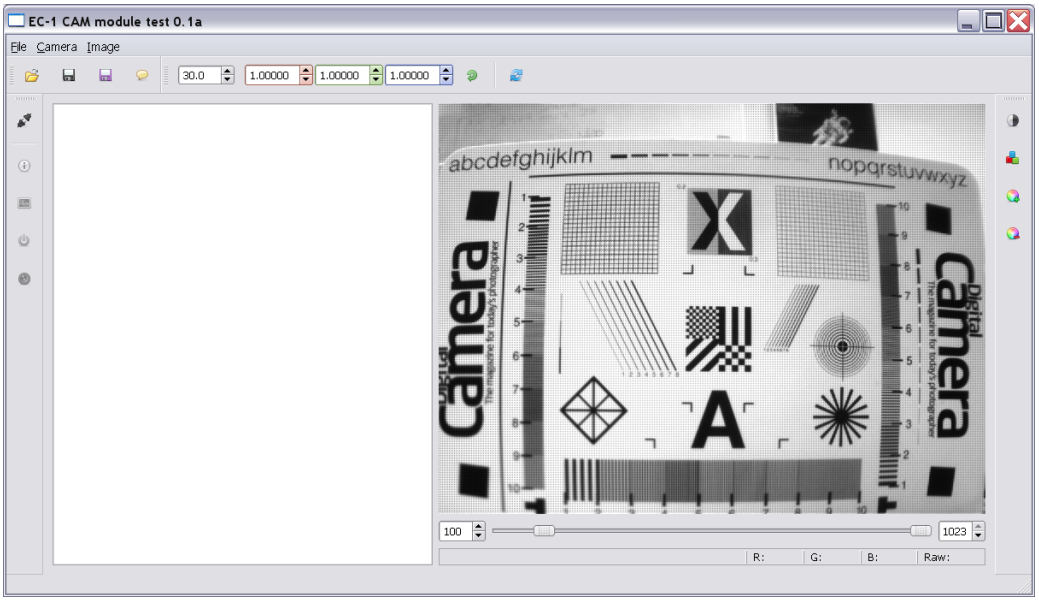

Figure 8. Screenshot of the PyCAM camera control software user interface. The white text area on the left displays debug output from the camera and from within the software itself.

send and receive packets. The main user interface includes controls to:

- configure the exposure and gain of the camera,
- read camera version and current status,
- read telemetry,
- trigger image capture and
- adjust the display range of the 10 bit image.

PyCAM also includes a linear de-mosaicing algorithm for the Bayer array that the MT9V011 sensor produces. For fast processing, the algorithm is implemented using parallel programming with the NumPy and SciPy libraries.

An automatic testing interface, illustrated in Figure 9, was added to PyCAM by Andreas Valdmann. This interface is used to automatically configure and trigger the camera through a series of loops. The PyFITS library is used to add information about test conditions to the images taken by the camera.

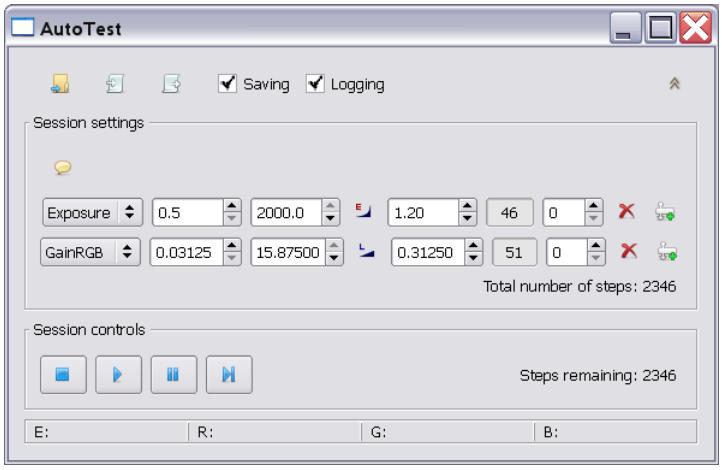

Figure 9. PyCAM automatic testing interface created by Andreas Valdmann.

5.2 Electrical tests

Basic imaging functionality and component connectivity were confirmed with the signal characteristics summarized in Table 5. At system startup clock signal stabilization to 90% of the final levels takes about 1.2 ms.

Table 5. Measured electrical characteristics for communication signals on the second camera prototype.

Signal	Rising edge (ns)	Falling edge (ns)	Low (V)	High (V)	Noise ($\pm$mV)
I^2C	110	50	-0.24	3.02	48.8
Pixel clock	5	5	-0.16	3.20	38.5
FSMC	6	5	-0.18	3.29	28.4
USART	48	51	-0.16	3.05	44.8

Power usage tests were run. Total power was measured using a laboratory power supply with an accuracy of ± 0.1 mA. Internal current consumption distribution was measured using the current-sense amplifiers on the camera module. The current-sense amplifier outputs were calibrated to a precision of ± 0.5 mA using the laboratory power supply. Measurements were done under different operating modes, showing power use through the different phases of camera operation.

Delays were inserted into the software to make the results more readable.

Figure 10 presents the resulting power usage in terms of current consumption.

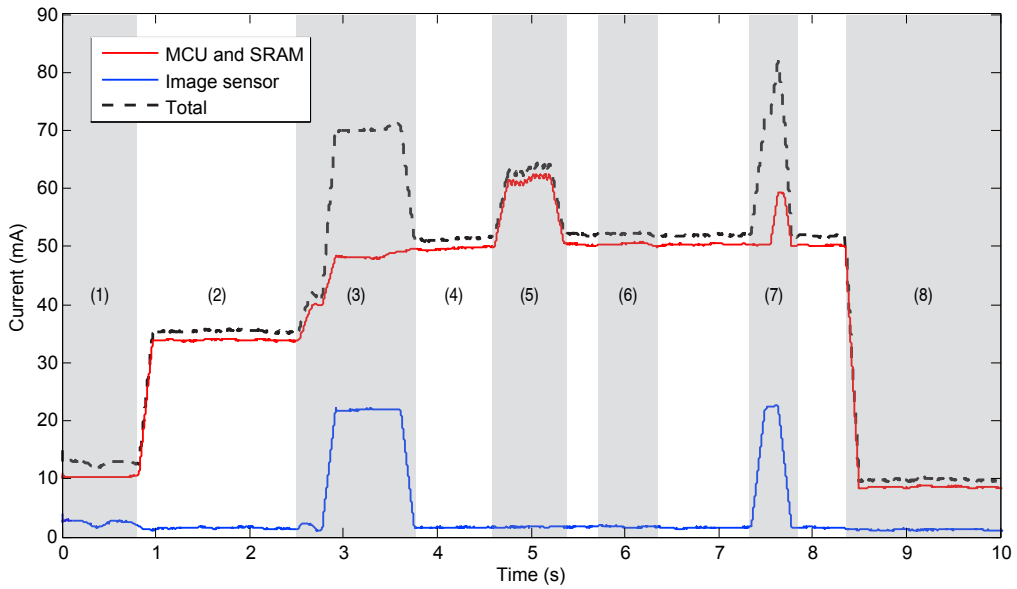

Figure 10. Current usage at 2.8 ± 0.2 V supply in different operating stages for the system prototype: (1) reset; (2) processor initialization; (3) sensor and external memory initialization; (4) MCU idle loop and sensor on standby; (5) 16 bit integer computation on data stored in external memory; (6) double precision computation on data stored in internal memory; (7) image capture; (8) standby.

Temperature tests were conducted using the prototype hardware version 2 and a temperature chamber. The prototype was connected to the computer using the USART interface to allow for recording of resets. The computer recorded 2 temperature readings, 2 power consumption readings, memory check results, and system reset types. An additional external temperature sensor was added and calibrated using the temperature chamber reading. The temperature chamber reading was also recorded manually. While the image sensor only supports a temperature range of -20 to +60 °C, tests were conducted in a wider range of -35 to +75°C.

The system performed without any memory errors, calculation errors, or resets. Power consumption only increased by 3 mW for the main board and 16 mW for the image sensor over the full range of the test.

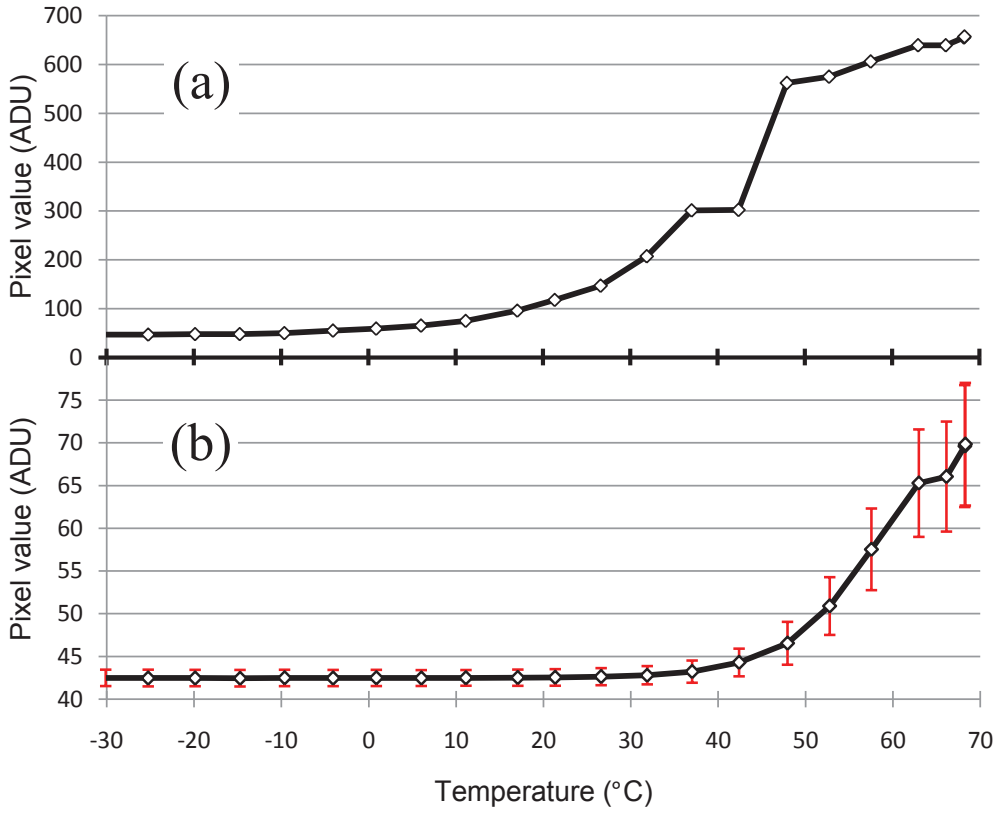

Figure 11. Results of image sensor temperature tests. (a) shows the maximum hot pixel value over the given temperature range. (b) shows the average dark current level with bias and noise for the same range.

Image sensor performance was also measured, by taking images at intervals of 5 °C with an exposure of 1 s. Figure 11a illustrates that hot pixels start having a measurable effect at around -5 °C. The bright hot pixels that occur from +30 °C onward, can have an effect on end mass imaging. However, hot pixel locations are constant, so this data can be uploaded to system ROM and used to correct the image during operation.

Noise also increases with temperature. Figure 11b shows the average dark current level including bias. Dark current starts to have a measurable effect at around +20 °C and increases significantly after +50 °C.

5.3 End mass imaging tests

For end mass imaging, initial test were done by imaging a known celestial body and comparing the relative result to the estimated magnitude of the end mass. Jupiter was chosen, because it was most visible at the time. The apparent magnitude of Jupiter was about -2.5^m [55]. Given that the estimated magnitude of the sunlit end mass is -7.3^m, the difference is 4.8^m. This means that the expected brightness of the tether end mass is about 83 times that of Jupiter at the time of the test.

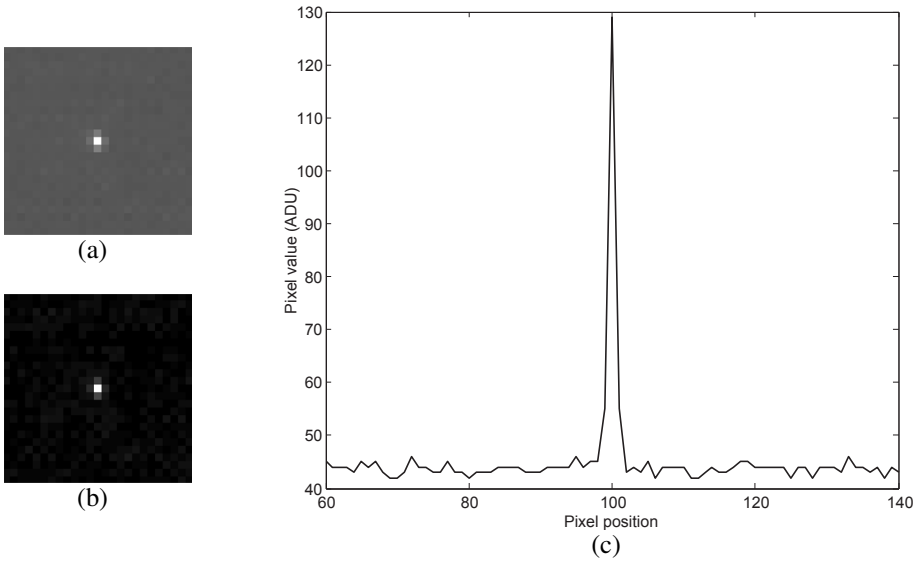

Figure 12. Jupiter test image at 100 ms exposure. Jupiter is clearly visible on the original magnified image (a). By subtracting the dark frame, we can see it even more clearly and remove some of the noise (b). The graph (c) shows the original pixel values for the row that Jupiter is visible on.

The camera was focused at around 3 m. Images were taken with exposures of 100 ms to 1 s and a gain of 1.0 in all 4 channels. The resulting image and graph in Figure 12, show that Jupiter signal strength at these settings is 90 ± 5 analog-to-digital units (ADUs).

Given the relative difference in brightness with the tether end mass, this demonstrates that the end mass will be visible even at much shorter exposures. Based on rotational speed and field of view calculations, 370 ms is available for end mass imaging during one rotation of tether deployment. Tether end mass image capture needs 4 images, this gives us a maximum of 92.5 ms per image. From this test, it is clear that an exposure of 10 ms would be enough to overexpose the end mass.

5.4 Simulated Earth imaging

Earth imaging from LEO is similar to taking a picture of clouds, sky and ground on Earth in direct sunlight conditions. To confirm the capability to take reasonably exposed images of Earth, a series of test images were captured in the described conditions. As a result of the early tests, it became clear that a ND filter with an optical density of 0.6 (25% transmittance) was needed in order to not overexpose the images at the fastest prototype exposure of 333 ns. In the final design image data transfer speed is increased, resulting in a minimum exposure of 68 ns. With the ND filter added, the results were much more promising as seen in Figure 13. Gain presets for correct color balance were also estimated from this.

Tests were also conducted with a sunlit neutral gray card. This allowed for more precise determination of gain presets for correct color balance.

5.5 Ongoing and planned tests

The camera system is currently being optically calibrated. The general characteristics for both the image sensor and lens have been provided by the manufacturers; however, we require exact information about the whole system, in order to accurately determine the end mass imaging capabilities of the camera. For this several tests are used. Absolute sensitivity and linearity are measured using an integrating sphere and by varying the gain and exposure of the camera. This will give us the relationships between light intensity, gain and exposure for each of the 4 types of pixels in the Bayer array. By varying the color gain separately for each of the 4 channels, color bleeding effects can also be measured.

Figure 13. A tone mapped HDR image of a sunlit scene taken with gain 1.0, 1.25 and 1.53 in the red, green and blue channels respectively. The exposures used were 333 ns, 504 ns and 672 ns (see appendix A for original images). [56]

Spectral sensitivity is measured using a monochromator in the wavelength region of 300 to 800 nm. The spectral sensitivity of the sensor is known; however, this test will measure the resulting characteristic curves for the whole system. In addition, dark and flat frames are captured to determine the relative differences between different areas of the image sensor and the dark current at different temperatures.

Many further tests are planned, before the camera can be launched into space. The most important of these tests are as follows:

- Radiation tests, to determine how well the software and image sensor can deal with various types and doses of radiation.
- Thermal vacuum tests, to determine the heat transfer through the lens assembly and how much this will affect both the image sensor and the MCU.

- Software unit tests need to be constructed for the final software. This will ensure that any last minute changes to the software will not break the system.
- Software fault injection will be used to simulate various error conditions and make sure the system is able to deal with these in the expected way.
- Hardware fault injection testing will be conducted, to guarantee system safety even if some communication lines or components fail.
- Various stress tests will be used to determine the points of failure under extreme conditions such as prolonged ultraviolet radiation and direct exposure to sunlight.
- Pictures of the actual end mass, lit by a light source similar to the expected conditions in orbit, will be taken. The data will be used to create reasonable camera presets for tether end mass imaging.

6 Results

A small, reliable and independent camera module was designed. The resulting hardware (see Figure 14 has the dimensions $43.3 \times 22 \times 44.2$ mm (W $\times$ H $\times$ D) and a mass of 30 g, which meets the requirements set by the initial ESTCube-1 budget. The aperture of the resulting optical system is 9 mm and the depth of field is 0.4 m to ∞.

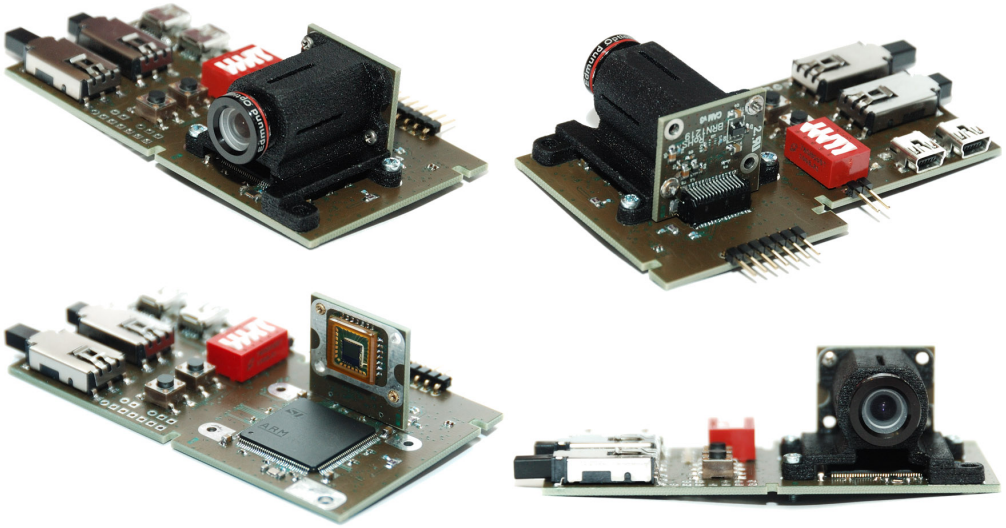

Figure 14. Photo of final camera hardware with debug wingboards.

Power consumption tests show that the power requirements were met with a peak power consumption of 238 mW, idle and processing power consumption of 145 mW, and standby power consumption of 30 mW. Based on these tests, it is also clear that overall power consumption can be lowered by disabling idle MCU peripherals and entering various low power and standby modes when idle for longer periods of time. Control over these low power modes can be given to external systems. Preliminary tests with final hardware show even lower power consumption. However, more tests need to be conducted after software has been finalized.

Temperature tests confirm, that the camera is able to operate reliably within the required operating range of -14 °C to +59 °C. Hot pixels might become visible

at high temperatures during tether end mass imaging; however, these can be corrected by recording hot pixel locations and parameters before launch. Sensor noise in the specified temperature range, is not an issue for either of the mission objectives.

A robust system is guaranteed by using recommended hardware design and layout to protect from interference. The hardware structure uses no plastics and consists mainly of aluminium, glass and FR-4 components. The camera control firmware features multiple levels of error protection and data redundancy. The use of FRAM provides additional data protection against the effects of radiation. In case of total software failure, the system also offers multiple ways of uploading new firmware. By having a totally independent system, any failure will not interfere with the rest of the satellite and the system can be safely shut down by EPS.

Flexibility is provided by the use of standard interfaces and a powerful processor. In addition to the USART interface used by ESTCube-1, the chosen MCU features

- $3 \times$ additional USART channels,
- $2 \times$ UART,
- $3 \times$ I^2C,
- $3 \times$ SPI,
- $2 \times$ CAN,
- $1 \times$ Ethernet and
- $1 \times$ USB 2.0 full-speed or high-speed interfaces.

Future applications of the system could use any combination of these interfaces for external control and communication.

By having the image sensor on a different board and using a standard M12 x 0.5 thread for the lens, both the image sensor and lens could be easily replaced for use in different applications.

Since the system features a powerful processor and is used only for short periods of time for image acquisition and processing, it is considered, that the MCU could also be utilized as a co-processor for CDHS on ESTCube-1. This might be useful for intensive calculations, such as attitude determination, freeing up the CDHS

to deal with other parts of the satellite. Furthermore, after the main mission, the bootloaders can be used to upload new firmware, providing us with a platform to test different algorithms and ideas without affecting the rest of the satellite.

By using a MCO pin of the MCU to clock the image sensor, more control is achieved over image sensor operating speed, without using extra components and additional power. Different image sensors, with different clock frequency requirements can easily be used, by simply changing the setup parameters in the firmware.

Based on current tests, the camera is capable of capturing both the tether end mass and Earth at reasonable parameters and speeds. For end mass imaging it can be seen, that the camera has enough time to capture multiple overexposed images, thus, increasing the probability of capturing the small bright end mass.

For Earth imaging, the combination of an ND filter, exposure bracketing and HDR gives the best chance of obtaining images at correct exposures. At a resolution of 1 km per pixel, Estonia should be clearly identifiable. An image capture rate of 30 fps results in the satellite moving about 8 arcseconds during the operation of the rolling shutter. This means that the shift in the image is about 248 meters or 25% of a pixel at an orbit of 700 km. Since the effect is cumulative over the whole frame, this does not affect our Earth imaging capabilities.

In addition to using lossless image compression, multiple algorithms have been designed to evaluate captured images and reduce the transfer size of images. The system provides both automatic and manual control over imaging parameters, to increase the chances of successfully capturing useful images.

Further tests have been planned and will be conducted to calibrate the optical system and confirm the findings of previous tests.

7 Summary

A small and independent camera system for ESTCube-1 tether end mass imaging and Earth imaging was developed and assembled. Detailed requirements analysis was conducted and both hardware and software were designed and iterated based on these constraints. The final design meets and exceeds all the power, volume, temperature and functional requirements.

A software design with novel image evaluation and processing algorithms has been outlined. These algorithms are used to reduce the amount of communication bandwidth used by the imaging system. In addition, the software design contains many redundancies and multiple levels of error correction in order to deal with soft and firm errors. Redundant bootloaders are provided for dealing with hard software errors. Moreover, this allows new firmware to be uploaded to the module once the main mission has been performed, thereby extending the usefulness of the satellite.

Using custom testing software, tests have been run to confirm that the developed hardware is capable of detecting the end mass in the required time frame and at distances from 0.4 to 10 m. Furthermore, it has been shown that the camera is able to image the Earth at a resolution of about 1 km per pixel. Measures have been taken in hardware and software to ensure correct exposure of images. Reliable operation in a wide range of temperatures has been confirmed and future tests have been planned to make sure the system can be operated safely under various extreme conditions.

The developed system is an easy to use stand-alone module, that provides many additional communications interfaces and possibilities. Therefore, it is flexible enough to be used in future satellite missions.

Currently, interest in the camera design has been expressed by the team of the Finnish satellite Aalto-1 [57, 58]. The camera module is also planned for use in multiple upcoming Tartu University and Tartu Observatory projects [59, 2].

8 Acknowledgements

I would like to thank my supervisors Tõnis Eenmäe, Viljo Allik and Ilmar Ansko, I have learned a lot from them. I would especially like to express my gratitude to Viljo Allik for sharing his knowledge and experience.

Many thanks to Ants Agu and Andreas Valdmann for being great team members and helping to get the camera system done and tested in time.

Thanks to Reimo Soosaar for providing all the 3D printed camera structures for development and testing.

I would also like to thank Tartu Observatory and the ESTCube-1 team for a very pleasant work environment and the team leaders Silver Lätt and Mart Noorma for doing such a good job on keeping everything on track.

Special thanks are due to Aivo Reinart for introducing me to the ESTCube project in the first place.

ESTCube-1 satelliidi kaamera alamsüsteemi disain
Henri Kuuste

9 Kokkuvõte

Eesti esimese tudengisatelliidi ESTCube-1 [1] teaduslikuks missiooniks on elektrilise päikesepurje tehnoloogia põhimõtte katsetamine Maa ionosfääri plasmas [2]. Selle saavutamiseks lennutatakse CubeSat standardil [4] põhinev ühikulise suurusega kuupsatelliit madalale polaarorbiidile. Peale satelliidi esialgset stabiliseerimist ja pildistamiseks Maa poole suunamist pannakse satelliit pöörlema kiirusega 1 pööre sekundis. Tekkiva tsentrifugaaljõu abil keritakse satelliidist välja 10 m pikkune mikrojuhe, millele antakse positiivne laeng. Seejärel mõõdetakse ionosfääri plasma ja laetud mikrojuhtme vastasmõjust tingitud satelliidi pöörlemiskiiruse muutust. [3]

Eksperimendi jälgimiseks ja kinnitamiseks töötati välja kaamerasüsteem, mis on võimeline kogu katse vältel tuvastama mikrojuhtme otsas asetsevat 12 mm läbimõõduga valget alumiiniumist otsamassi. Lisaks kasutatakse sama kaamera moodulit teaduse populariseerimise eesmärkidel Maast ja loodetavasti ka Eestist piltide tegemiseks. Samuti oli oluline, et loodud süsteem oleks lihtsasti taaskasutatav ka teistes projektides.

Antud töö peamisteks eesmärkideks oli:

- analüüsida kaamera alamsüsteemi nõudeid,
- koostada nõuetele vastav ja taaskasutatav riistvara,
- testida selle funktsionaalsust ja töökindlust,
- ning kirjeldada loodava süsteemi tarkvaralist ülesehitust.

Töö viidi läbi pooleteise aasta jooksul ning koostatud kaamera moodul ületas kõiki esitatud nõudeid. Tuginedes teostatud testide tulemustele, võime olla kindlad, et kaamera on suuteline mikrojuhtme otsamassi tuvastama 0,4 kuni 10 m kauguselt, ning pildistama Maad lahutusega 1 km piksli kohta.

Töös kirjeldatud tarkvara sisaldab uudseid algoritme, millega on võimalik suurendada kvaliteetsete piltide saamise tõenäosust ja vähendada Maale saadetavate

andmete hulka. Satelliidi missiooni olemuse tõttu on kaamerale esitatavad reaalajasüsteemi nõuded väga ranged. Riskide alandamiseks on loodud tarkvaras mitu veahalduse taset ning kaks võimalust uue tarkvara paigaldamiseks. Vähendamaks kosmilise kiirguskeskkonna võimalikku mõju kaamera elektroonikale ja tarkvarale on kaamera juhtimistarkvaras rakendatud mitmed vigade kaitse meetmed.

Töö käigus valmis kaks riistvara prototüüpi, lõplik kaamera riistvara, juhtimistarkvara prototüüp ja testimistarkvara lahendus. Täiendavalt töötati välja edasiste testide plaanid, mille käigus kalibreeritakse kaamera optika ning testitakse süsteemi töökindlust väga äärmuslikes tingimustes.

Loodud kaamera on iseseisev moodul, mida erinevate liideste abil on võimalik lisada ka tulevastesse satelliidiprojektidesse. Hetkeseisuga on kaamera disaini vastu huvi üles näidanud Soome satelliidi Aalto-1 meeskond [57, 58] ning sama moodulit on plaanis kasutada mitmes Tartu Ülikooli ja Tartu Observatooriumi projektis [59, 2].

References

[1] "Estonian student satellite project," http://www.estcube.eu (accessed 25 May 2012).

[2] "Electric Solar Wind Sail (E-sail) website," http://www.electric-sailing.fi/index.html (accessed 25 May 2012).

[3] P. Janhunen, P. K. Toivanen, J. Polkko, S. Merikallio, P. Salminen, E. Haeggstrom, H. Seppanen, R. Kurppa, J. Ukkonen, S. Kiprich, G. Thornell, H. Kratz, L. Richter, O. Kromer, R. Rosta, M. Noorma, J. Envall, S. Latt, G. Mengali, A. A. Quarta, H. Koivisto, O. Tarvainen, T. Kalvas, J. Kauppinen, A. Nuottajarvi, and A. Obraztsov, "Invited article: Electric solar wind sail: Toward test missions," Review of Scientific Instruments **81**, 111301 –111301–11 (2010).

[4] "CubeSat Design Specification Rev. 12," California State Polytechnic University (2009). www.cubesat.org/images/developers/cds_rev12.pdf (accessed 26 May 2012).

[5] G. B. Ballı, "Micro-satellite camera design," Ph.D. thesis, Graduate School of Natural and Applied Sciences of Middle East Technical University (2003). http://etd.lib.metu.edu.tr/upload/1043769/index.pdf (accessed 26 May 2012).

[6] K. Gulzar, "Camera Design for Pico and Nano Satellite Applications," Master's thesis, Luleå University of Technology (2009). http://epubl.ltu.se/1653-0187/2010/013/ (accessed 26 May 2012).

[7] http://www.space.t.u-tokyo.ac.jp/cubesat/mission/launch/index-e.html (accessed 21 May 2012).

[8] http://www.space.t.u-tokyo.ac.jp/cubesat/mission/Vlaunch/index-e.html (accessed 21 May 2012).

[9] Y. Tsuda, N. Sako, T. Eishima, T. Ito, Y. Arikawa, N. Miyamura, A. Tanaka, and S. Nakasuka, "University of Tokyo's CubeSat Project - Its Educational

and Technological Significance," in "The 15th Annual AIAA/USU Conference on Small Satellites," (Logan, Utah, 2001), pp. 13–16.

[10] Y. Tsuda, N. Sako, T. Eishima, T. Ito, Y. Arikawa, N. Miyamura, K. Kanairo, S. Ukawa, S. Ogasawara, and S. Ishikawa, "University of Tokyo's CubeSat "XI" as a student-built educational pico-satellite - Final design and operation plan," in "The 23rd International Symposium of Space Technology and Science," , vol. 2 (2002), vol. 2, pp. 1372–1377.

[11] "University of Tokyo CubeSat project page," `http://www.space.t.u-tokyo.ac.jp/cubesat/index-e.html` (accessed 21 May 2012).

[12] "XI-V Twitter feed," `http://twitter.com/#!/XI_V/media/grid` (accessed 21 May 2012).

[13] "Earth pictures from XI-V #1," `http://www.ne.jp/asahi/hamradio/je9pel/xivpict1.htm` (accessed 21 May 2012).

[14] "Cute-1.7 + APD II Project – Launch and Operation," `http://lss.mes.titech.ac.jp/ssp/cute1.7/lanunchandoperation_e.html` (accessed 21 May 2012).

[15] H. Ashida, K. Fujihashi, S. Inagawa, Y. Miura, K. Omagari, N. Miyashita, S. Matunaga, T. Toizumi, J. Kataoka, and N. Kawai, "Design of Tokyo Tech nano-satellite Cute-1.7+APD II and its operation," Acta Astronautica **66**, 1412–1424 (2010).

[16] N. Miyashita, M. Iai, K. Omagari, K. Imai, H. Yabe, K. Miyamoto, T. Iljic, T. Usuda, K. Fujiwara, S. Masumoto, Y. Konda, S. Sugita, T. Yamanaka, K. Konoue, and S. Matunaga, "Development of Nano-Satellite Cute-1 . 7 + APD and Its Current Status," in "The 56th International Astronautical Congress," (Fukuoka, 2005).

[17] "Cute-1.7 + APD II Project – OnBoard Camera Image Gallery," `http://lss.mes.titech.ac.jp/ssp/cute1.7/gallery_camera_e.html` (accessed 21 May 2012).

[18] "AMSAT Satellite Detail – PRISM," http://www.amsat.org/amsat-new/satellites/satInfo.php?satID=119 (accessed 21 May 2012).

[19] M. Komatsu, "University of Tokyo Nano Satellite Project "PRISM"," in "26th International Symposium on Space Technology and Science," (Hamamatsu, 2008).

[20] "PRISM Project Image Gallery," http://www.space.t.u-tokyo.ac.jp/prism_old/gallery-e.html (accessed 21 May 2012).

[21] K. Shimizu, "University of Tokyo Nano Satellite Project "PRISM"," in "27th International Symposium on Space Technology and Science," (Tsukuba, 2009), pp. 4–9.

[22] "AMSAT Satellite Detail – AAU Cubesat," http://www.amsat.org/amsat-new/satellites/satInfo.php?satID=102 (accessed 21 May 2012).

[23] L. Alminde, M. Bisgaard, D. Bhanderi, and J. D. Nielsen, "Experience and methodology gained from 4 years of student satellite projects," in "Recent Advances in Space Technologies, 2005. RAST 2005. Proceedings of 2nd International Conference on," (2005), pp. 94–99.

[24] L. Alminde, M. Bisgaard, D. Vinther, T. Viscor, and K. Ostergard, "Educational value and lessons learned from the AAU-CubeSat project," in "Recent Advances in Space Technologies, 2003. RAST '03. International Conference on. Proceedings of," (2003), pp. 57–62.

[25] M. Borgeaud, N. Scheidegger, M. Noca, G. Roethlisberger, F. Jordan, T. Choueiri, and N. Steiner, "SwissCube: The First Entirely-Built Swiss Student Satellite with an Earth Observation Payload," in "Small Satellite Missions for Earth Observation," , R. Sandau, H.-P. Roeser, and A. Valenzuela, eds. (Springer Berlin Heidelberg, 2010), pp. 207–213.

[26] M. Noca, F. Jordan, N. Steiner, T. Choueiri, F. George, G. Roethlisberger, N. Scheidegger, H. Peter-contesse, M. Borgeaud, R. Krpoun, and H. Shea,

"Lessons Learned from the First Swiss Pico-Satellite : SwissCube," Science (2009).

[27] "AMSAT Satellite Detail – SwissCube," http://www.amsat.org/amsat-new/satellites/satInfo.php?satID=126 (accessed 21 May 2012).

[28] "SwissCube project main page," http://swisscube.epfl.ch/ (accessed 21 May 2012).

[29] A. Scholz, J. Giesselmann, and C. Duda, "CubeSat Technical Aspects," in "55th International Astronautical Congress," (Vancouver, 2004).

[30] "AMSAT Satellite Detail – COMPASS-1," http://www.amsat.org/amsat-new/satellites/satInfo.php?satID=114 (accessed 21 May 2012).

[31] A. Scholz, W. Ley, B. Dachwald, J. J. Miau, and J. C. Juang, "Flight results of the COMPASS-1 picosatellite mission," Acta Astronautica **67**, 1289–1298 (2010).

[32] "Canadian Advanced Nanospace eXperiment Program," http://en.wikipedia.org/wiki/Canadian_Advanced_Nanospace_eXperiment_Program (accessed 21 May 2012).

[33] "Nanosatellite Launch System 4," http://www.utias-sfl.net/NLS-4/ (accessed 21 May 2012).

[34] D. Rankin, D. D. Kekez, R. E. Zee, F. M. Pranajaya, D. G. Foisy, and A. M. Beattie, "The CanX-2 nanosatellite: Expanding the science abilities of nanosatellites," Acta Astronautica **57**, 167–174 (2005).

[35] K. Sarda, S. Eagleson, E. Caillibot, C. Grant, D. Kekez, F. Pranajaya, and R. E. Zee, "Canadian advanced nanospace experiment 2: Scientific and technological innovation on a three-kilogram satellite," Acta Astronautica **59**, 236–245 (2006).

[36] C. Kurtulus, T. Baltaci, M. Ulusoy, B. T. Aydm, B. Tutkun, G. Inalhan, N. L. O. Cetiner-Yildirim, T. B. Karyot, C. Yarim, F. O. Edis, and Others, "iTU-pSAT I: Istanbul Technical University Student Pico-Satellite Program," in "Recent Advances in Space Technologies, 2007. RAST'07. 3rd International Conference on," (IEEE, 2007), pp. 725–732.

[37] G. İnalhan, E. Başkaya, and E. Koyuncu, "ITU pSAT II ADCS : Getting Ready for Lauch," in "8th Annual CubeSat Developers' Workshop," (2011).

[38] R. Soosaar and J. Viru, "Phase B report of ESTCube-1 Environment Subsystem," Tech. rep., University of Tartu (2010).

[39] "Polar satellite launch vehicle user's manual," Issue 5, Indian Space Research Organisation (2007).

[40] I. Sünter, "Radiation tolerant hardware design for ESTCube-1 Command and Data Handling System," Bachelor thesis, University of Tartu (2011).

[41] P. Liias (2012). Personal communication.

[42] T. Eenmäe, V. Allik, and I. Ansko, "ESTCube-1 Camera Subsystem Phase B report," Tech. rep., University of Tartu (2010).

[43] T. Peet (2012). Personal communication.

[44] P. Janhunen (2010). Personal communication.

[45] "STAR-1000 – 1 M Pixel Radiation - Hard CMOS image sensor," Tech. rep., Cypress Semiconductor (2005). `http://www.onsemi.com/pub_link/Collateral/NOIS1SM1000A-D.PDF` (accessed 26 May 2012).

[46] K. E. Gustafsson, "EMC Design," (Nokia, 2001).

[47] "Printed-Circuit-Board Layout for Improved Electromagnetic Compatibility," Tech. Rep. October, Texas Instruments (1996). `http://www.ti.com/lit/an/sdya011/sdya011.pdf` (accessed 26 May 2012).

[48] C. Troise, "AN1709: EMC design guide for ST microcontrollers," Tech. rep., STMicroelectronics (2003). http://www.st.com/internet/com/TECHNICAL_RESOURCES/TECHNICAL_LITERATURE/APPLICATION_NOTE/CD00004479.pdf (accessed 26 May 2012).

[49] "MT9V011: 1/4-Inch VGA Digital Image Sensor," Tech. rep., Aptina Imaging Corporation (2009). http://www.aptina.com/assets/downloadDocument.do?id=493 (accessed 26 May 2012).

[50] "DS6697: ARM-based 32-bit MCU, 150DMIPs, up to 1MB Flash/128+4KB RAM, crypto, USB OTG HS/FS, Ethernet, 17 TIMs, 3 ADCs, 15 comm. interfaces and camera," Tech. Rep. June, STMicroelectronics (2011). http://www.st.com/internet/com/TECHNICAL_RESOURCES/TECHNICAL_LITERATURE/DATASHEET/CD00263874.pdf (accessed 26 May 2012).

[51] "RM0033: STM32F205xx, STM32F207xx, STM32F215xx and STM32F217xx advanced ARM-based 32-bit MCUs," Tech. Rep. April, STMicroelectronics (2011). http://www.st.com/internet/com/TECHNICAL_RESOURCES/TECHNICAL_LITERATURE/REFERENCE_MANUAL/CD00225773.pdf (accessed 26 May 2012).

[52] "AN3430: How to achieve the lowest current consumption with STM32F2xx," Tech. Rep. August, STMicroelectronics (2011). http://www.st.com/internet/com/TECHNICAL_RESOURCES/TECHNICAL_LITERATURE/APPLICATION_NOTE/DM00033348.pdf (accessed 26 May 2012).

[53] "AN3320: Getting started with STM32F20xxx 21xxx MCU hardware development," Tech. Rep. August, STMicroelectronics (2011). http://www.st.com/internet/com/TECHNICAL_RESOURCES/TECHNICAL_LITERATURE/APPLICATION_NOTE/CD00292095.pdf (accessed 26 May 2012).

[54] "1M x 16 high-speed asynchronous CMOS static RAM with 3.3V supply," Tech. rep., Integrated Silicon Solution, Inc. (2006). http://www.issi.com/pdf/61WV102416ALL.pdf (accessed 26 May 2012).

[55] "U.S. Naval Observatory," http://aa.usno.navy.mil/data/docs/ssconf.php (accessed 7 January 2012).

[56] A. Valdmann (2012). Personal communication.

[57] J. Envall (2011). Personal communication.

[58] "Aalto-1 – Wikipedia," http://en.wikipedia.org/wiki/Aalto-1 (accessed 26 May 2012).

[59] "QB50, an international network of 50 CubeSats for multi-point, in-situ measurements in the lower thermosphere and re-entry research," https://www.qb50.eu (accessed 26 May 2012).

Appendices

Appendix A Earth imaging results

Figure 15. Earth imaging test taken at an exposure of 333 ns.

Figure 16. Earth imaging test taken at an exposure of 502 ns.

Figure 17. Earth imaging test taken at an exposure of 672 ns.

Appendix B Photos of hardware iterations

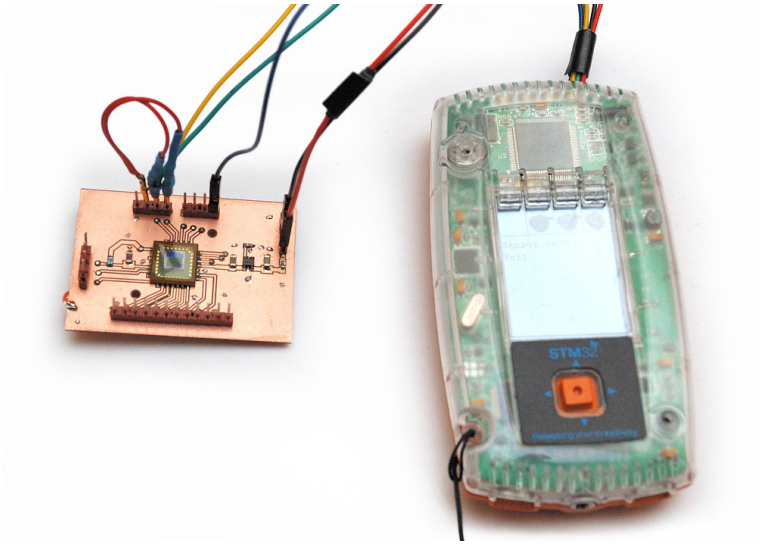

Figure 18. First sensor tests with an STM32 development kit.

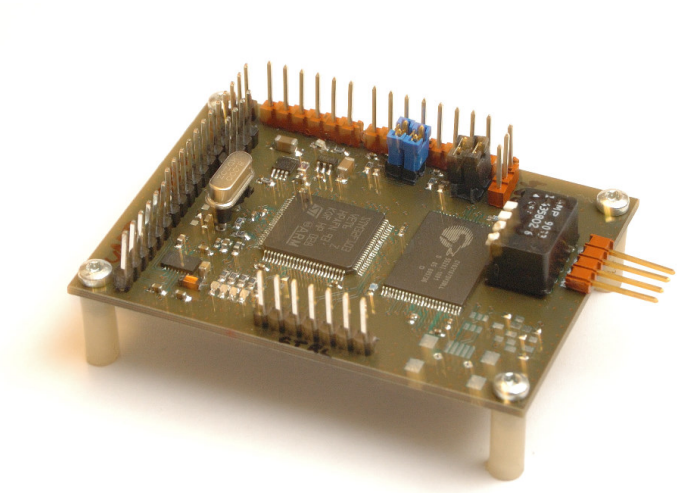

Figure 19. First MCU and SRAM tests using the same processor as CDHS.

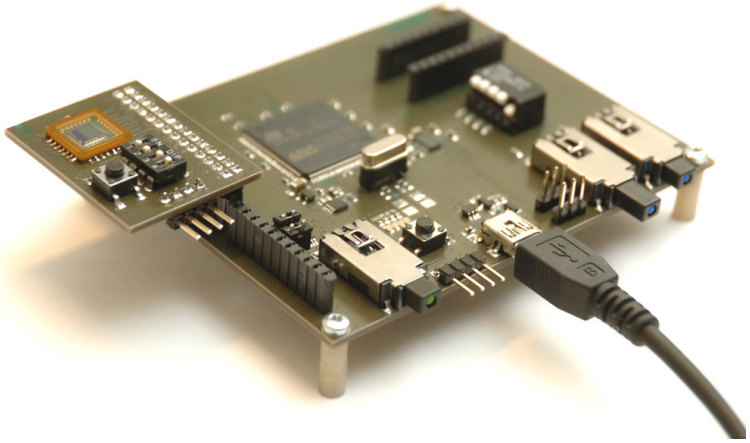

Figure 20. Second camera prototype without optics. This was actually the first complete working system. Many connectors are provided for easy access with measurement devices.

Figure 21. A test of how the final hardware would look and fit together, using two layer PCBs.

Appendix C Main PCB schematics

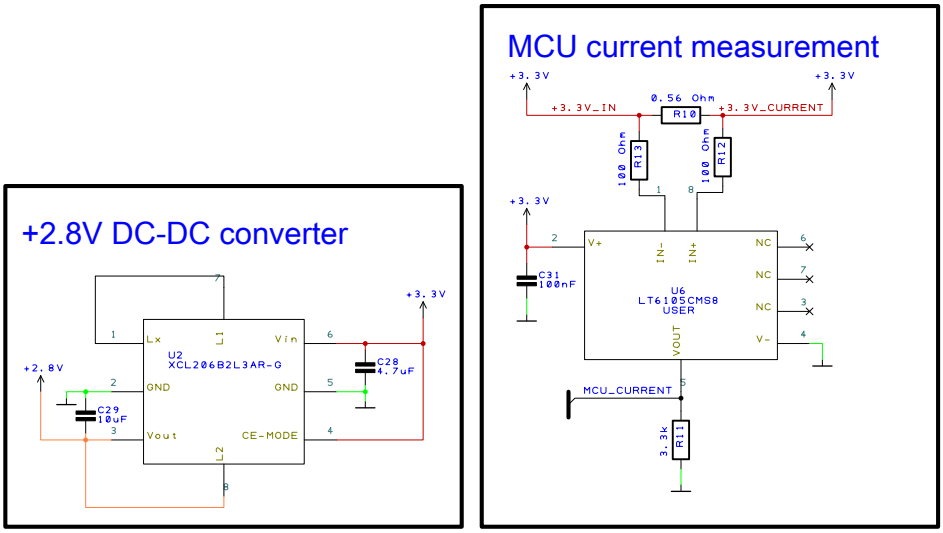

Figure 22. Power supply and current measurement.

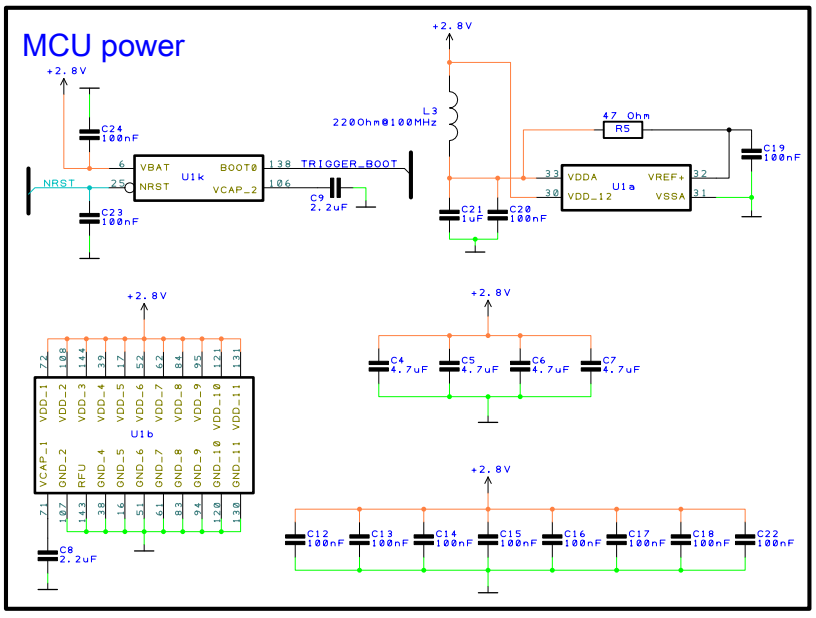

Figure 23. Microcontroller power.

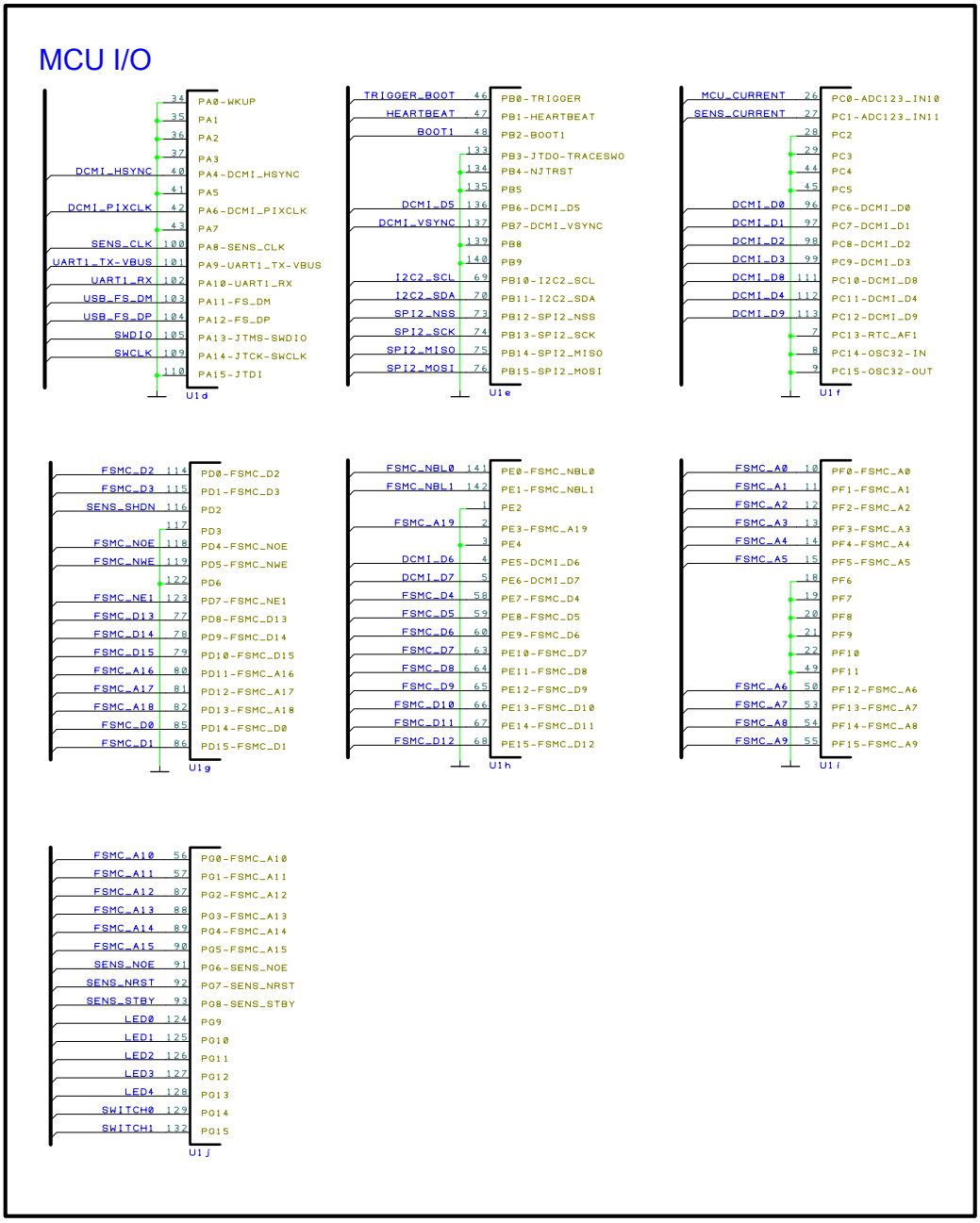

Figure 24. Microcontroller input/output connections.

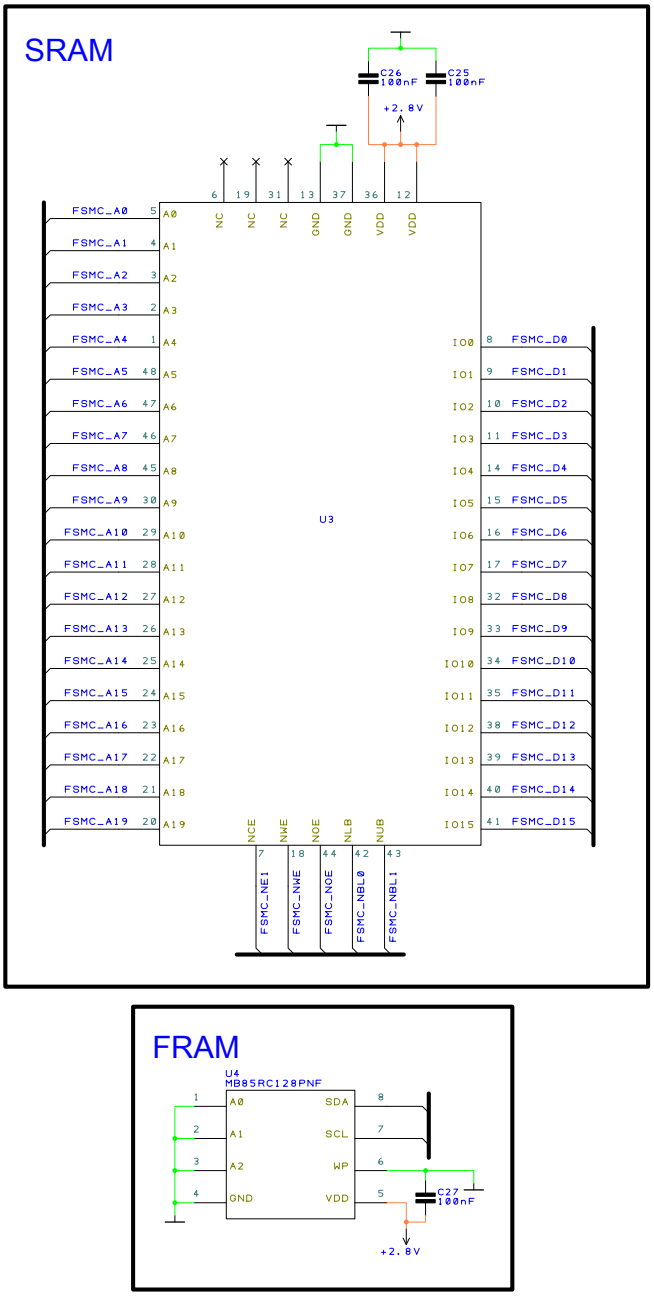

Figure 25. Memory modules.

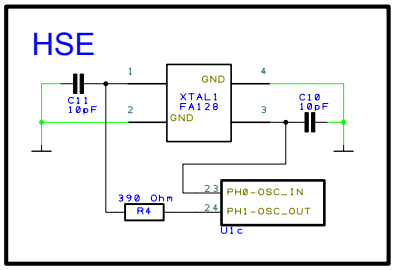

Figure 26. High-speed external clock.

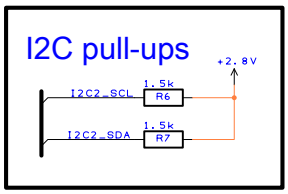

Figure 27. I^{2}C bus pull-ups.

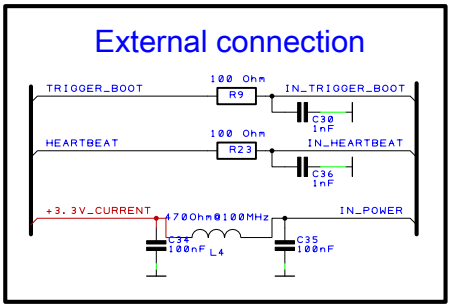

Figure 28. Satellite stack connections.

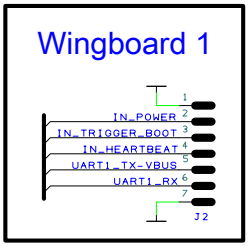

Figure 29. Wingboard for stack connections.

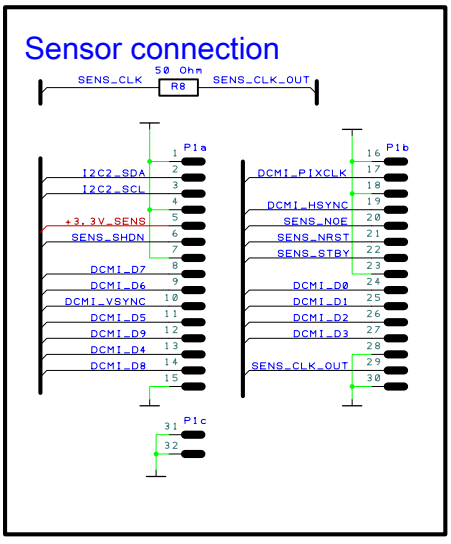

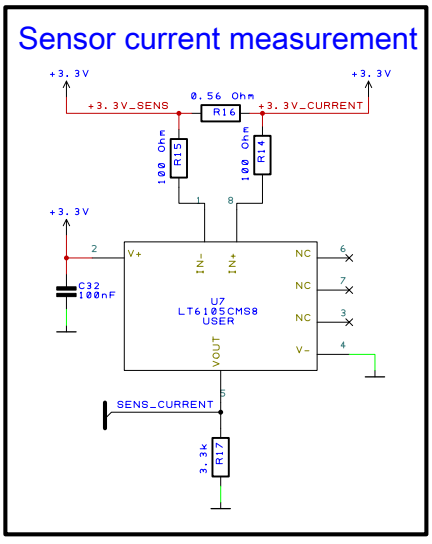

Figure 30. Sensor connections.

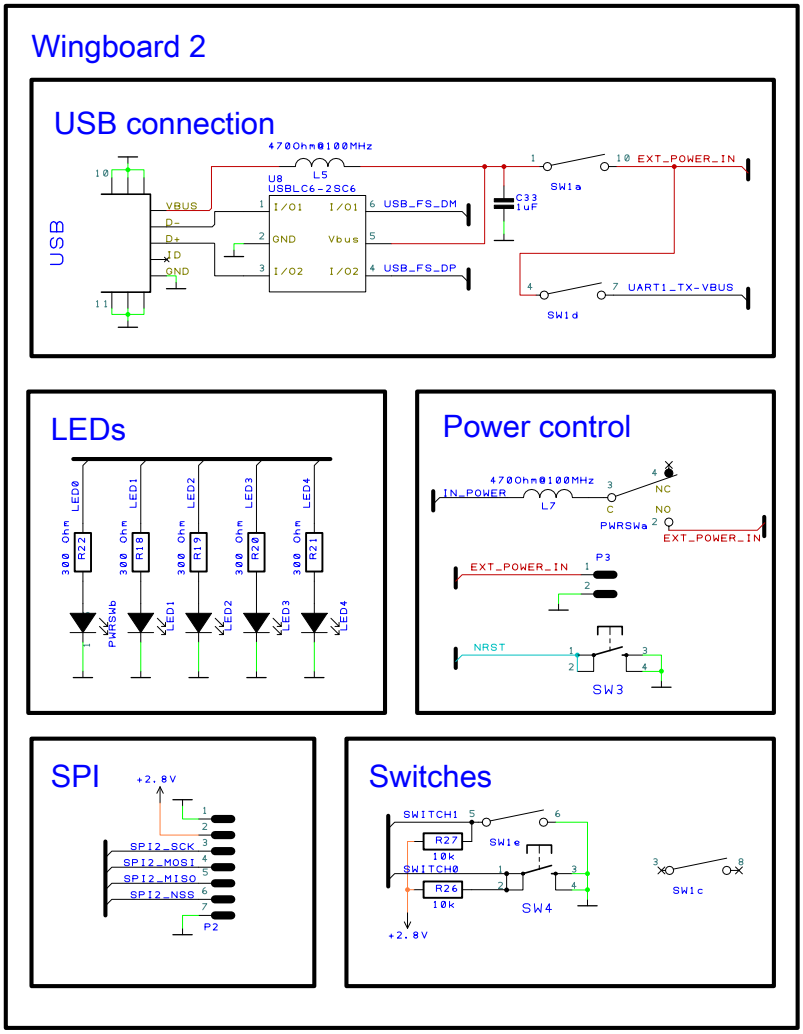

Figure 31. Debug wingboard.

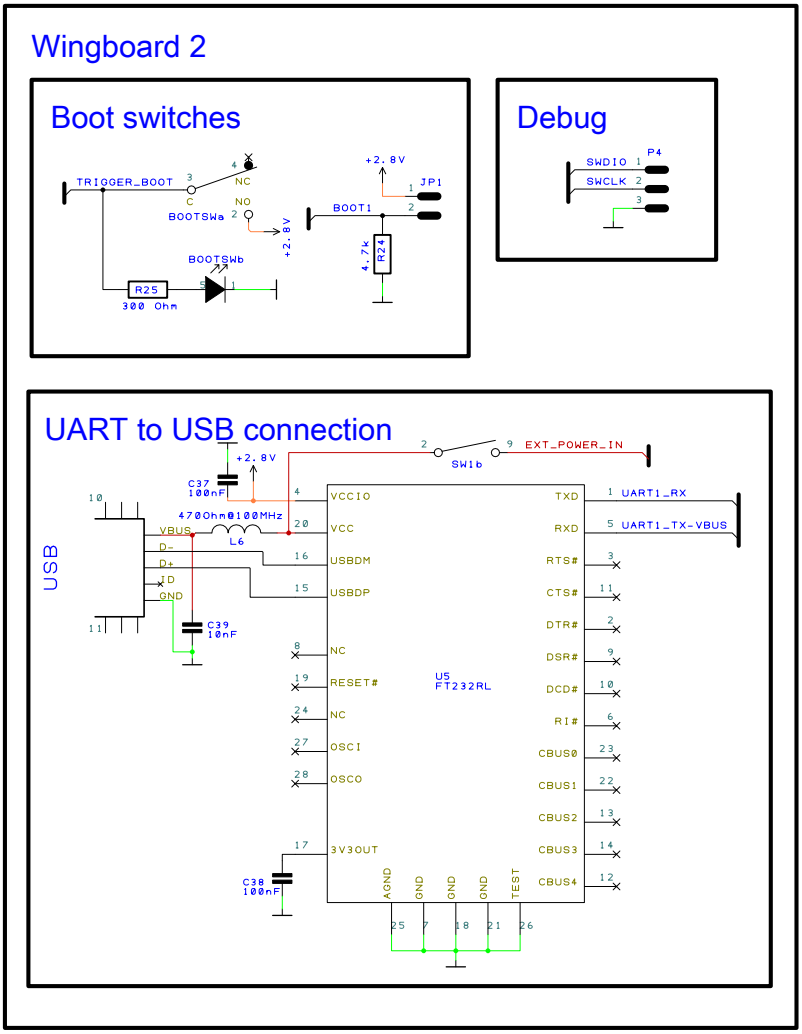

Figure 32. Debug wingboard.

Appendix D Sensor schematics

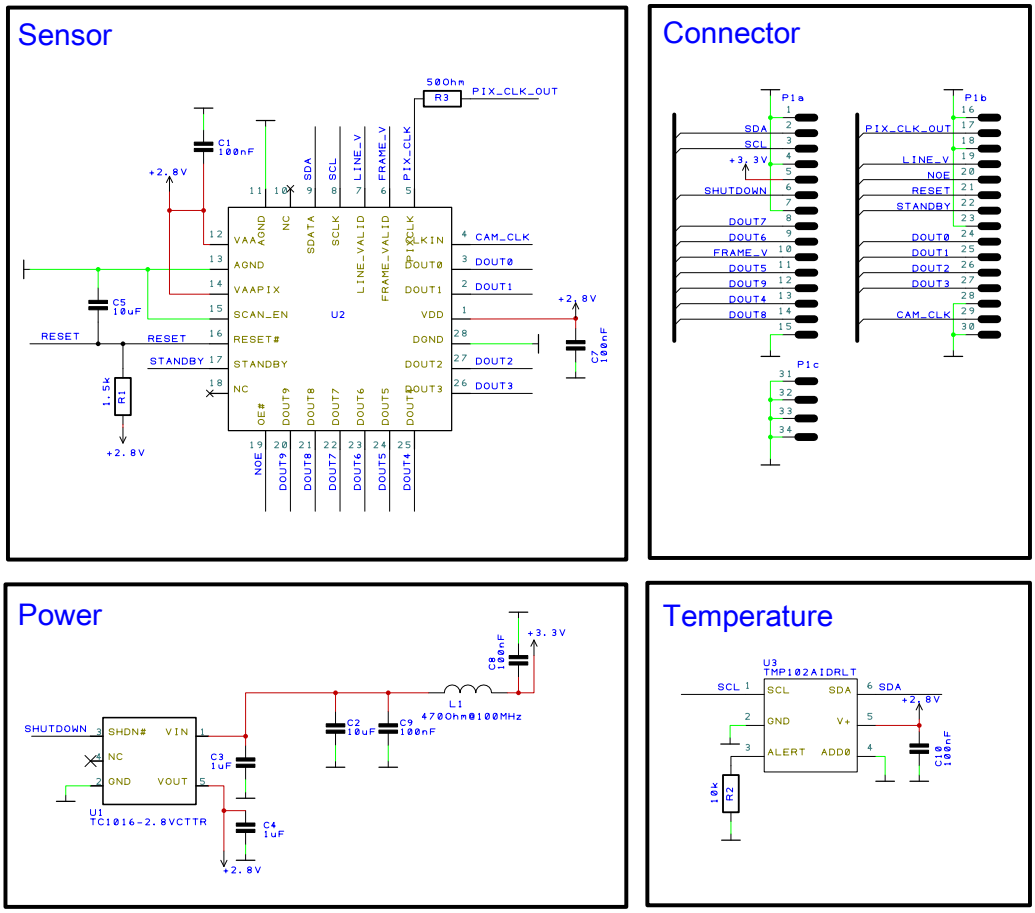

Figure 33. Sensor board schematics.

Appendix E Main PCB layout

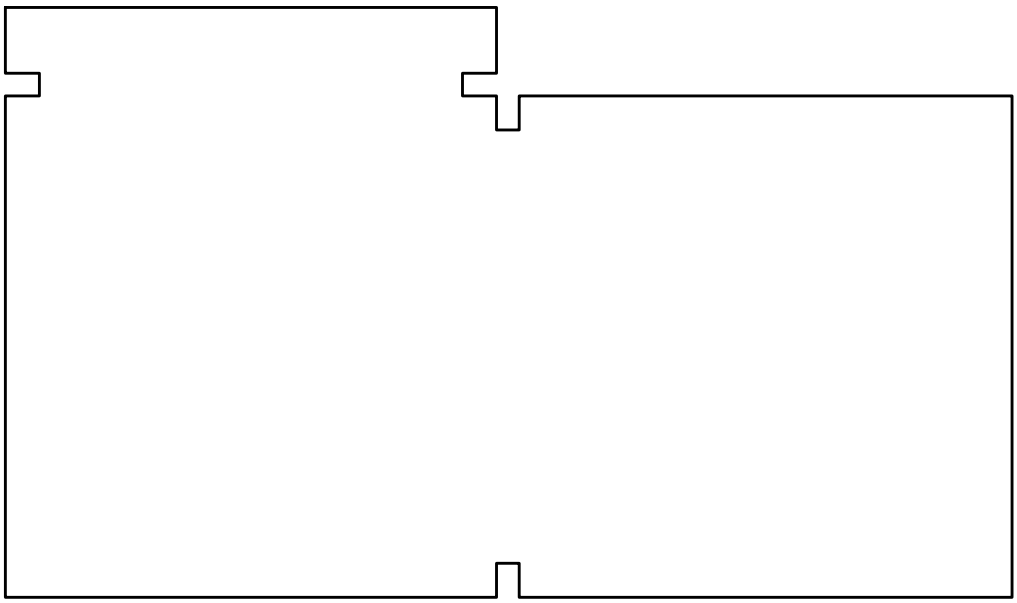

Figure 34. Board outline (scale 1.5).

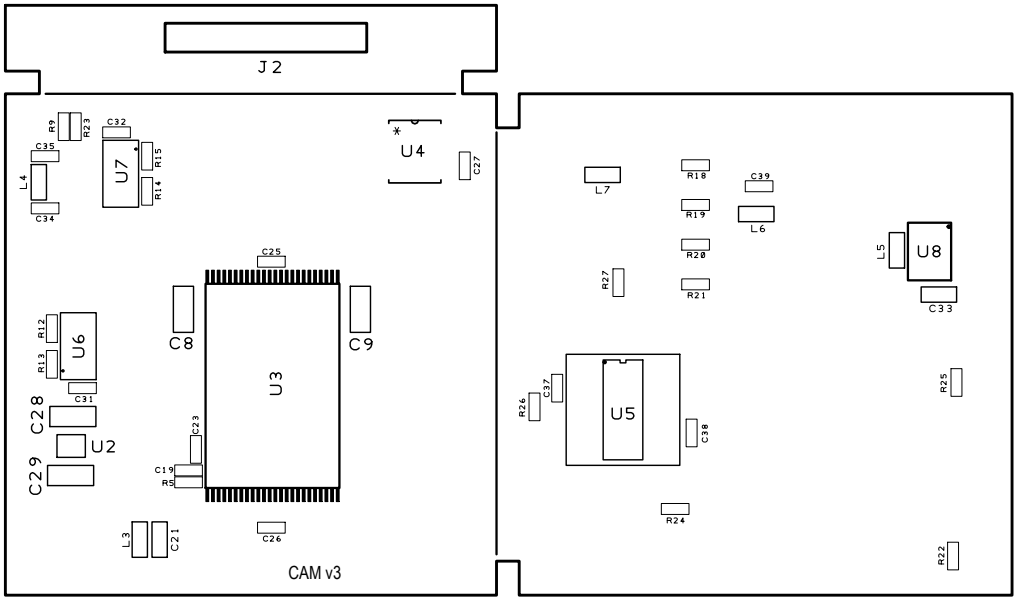

Figure 35. Top silkscreen (scale 1.5).

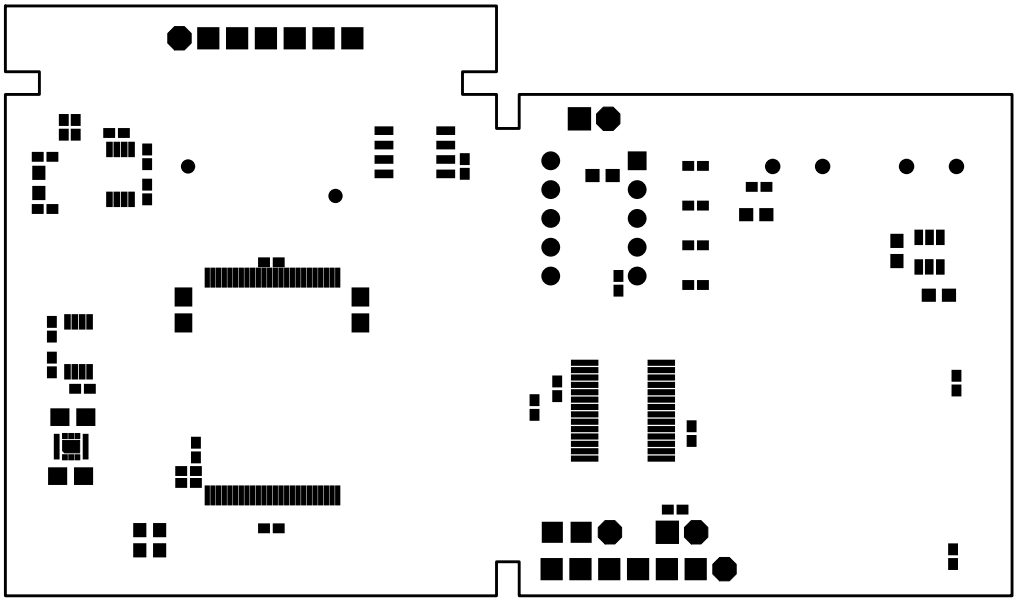

Figure 36. Top mask (scale 1.5).

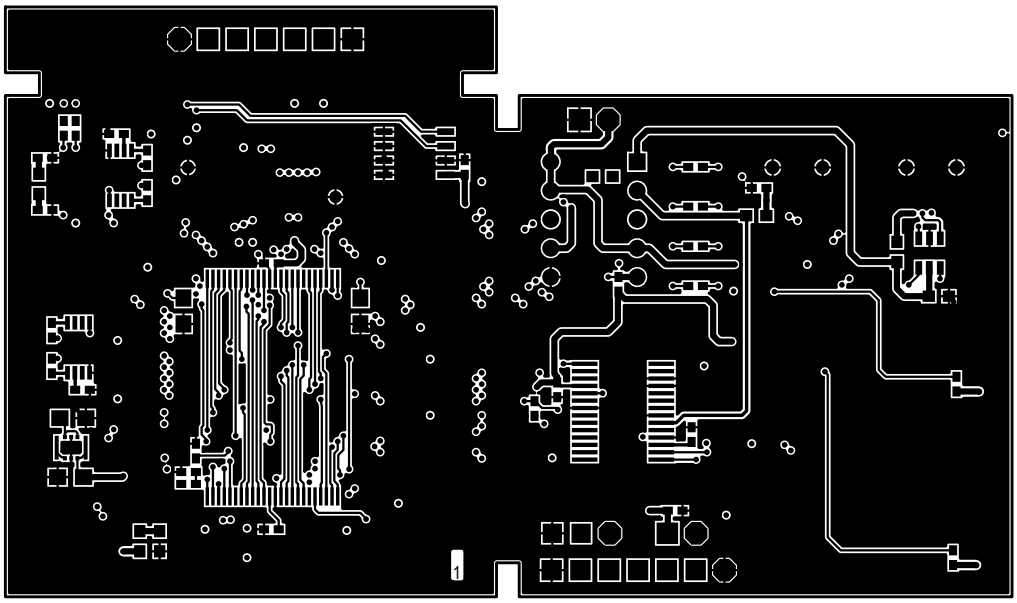

Figure 37. Top copper (scale 1.5).

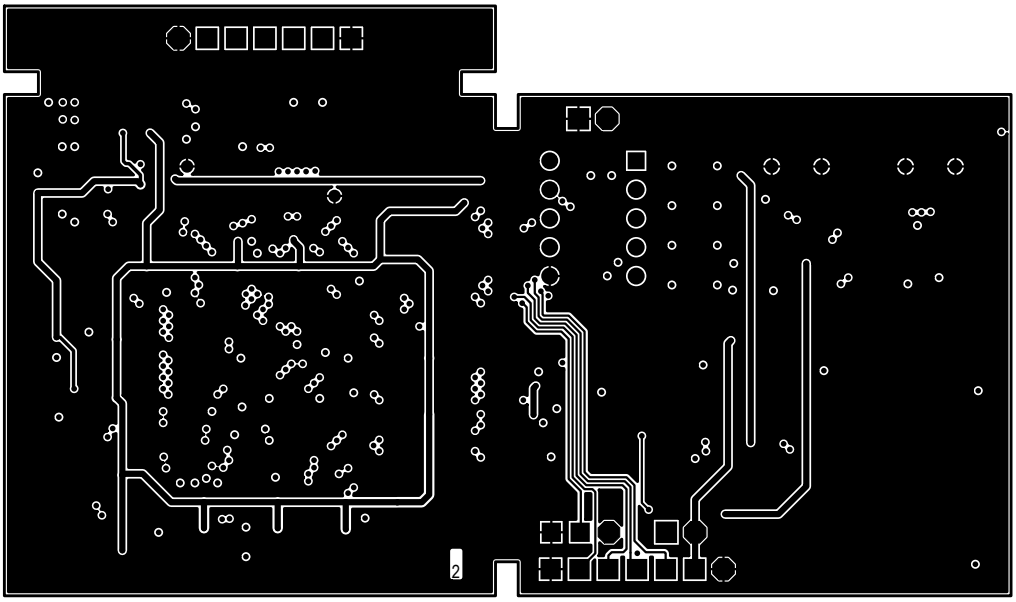

Figure 38. Inner 1 - power (scale 1.5).

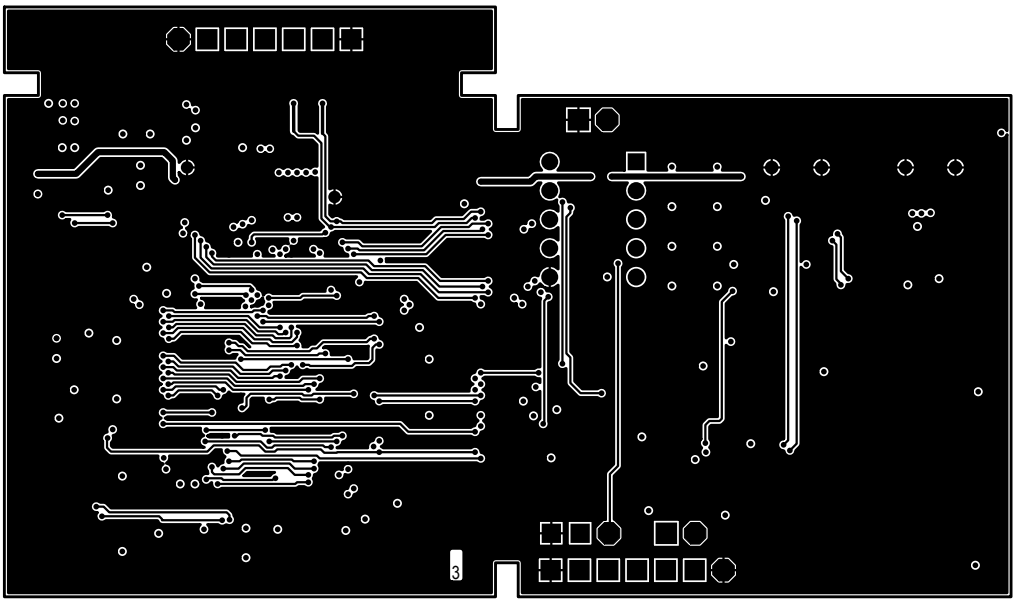

Figure 39. Inner 2 (scale 1.5).

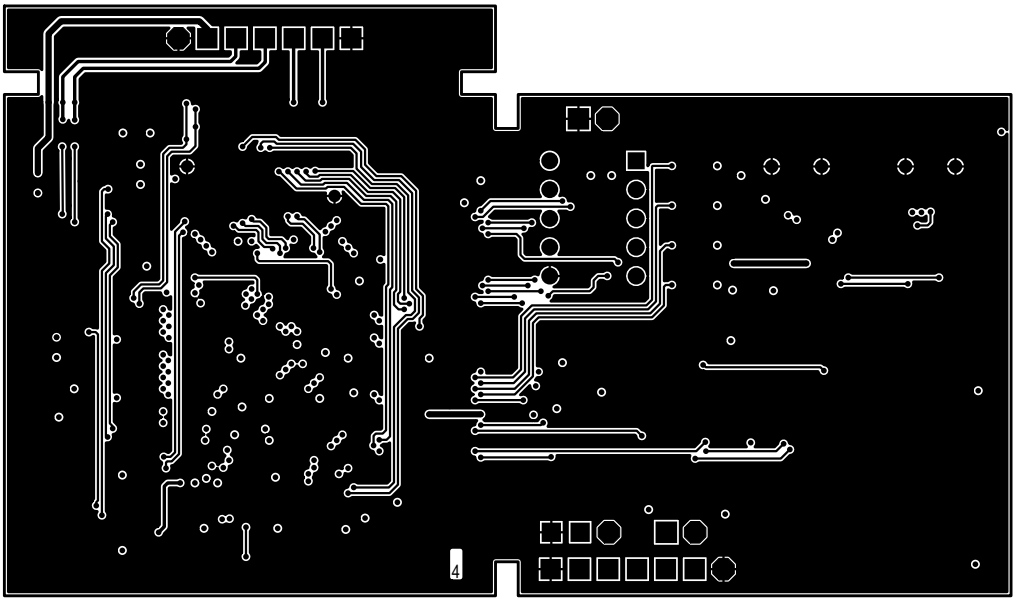

Figure 40. Inner 3 (scale 1.5).

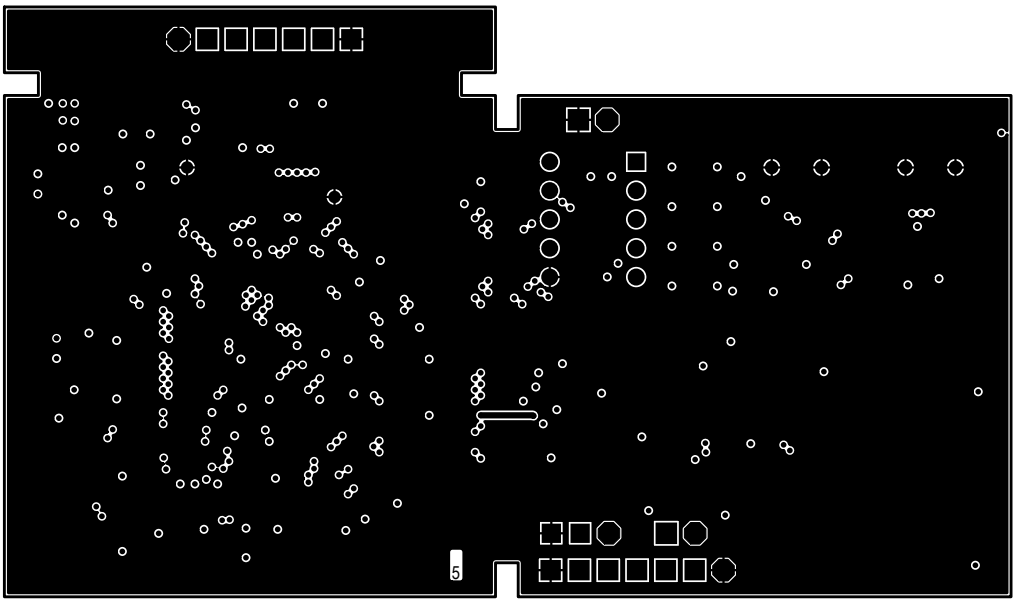

Figure 41. Inner 4 - ground (scale 1.5).

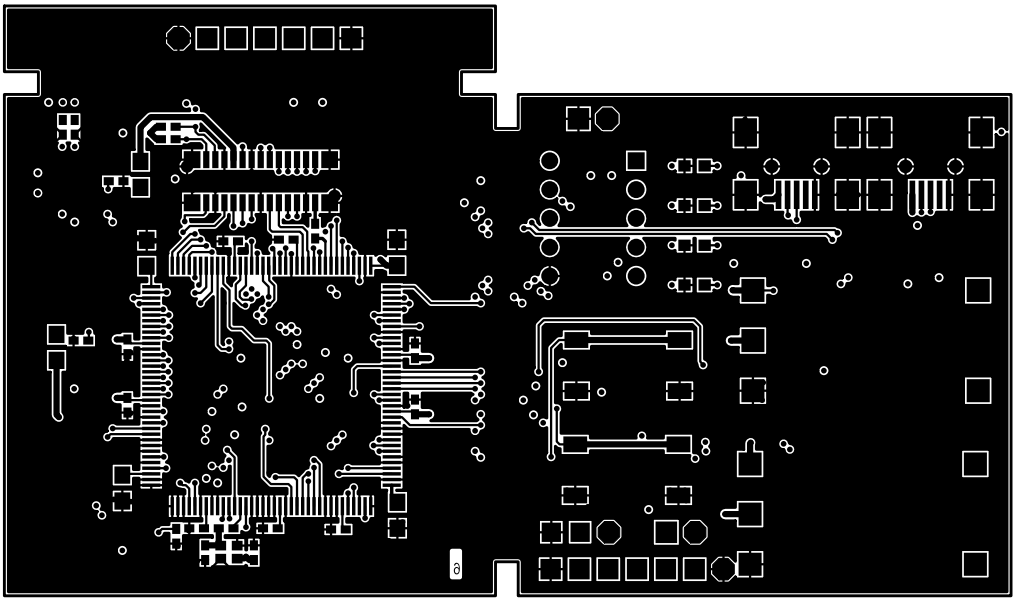

Figure 42. Bottom copper (scale 1.5).

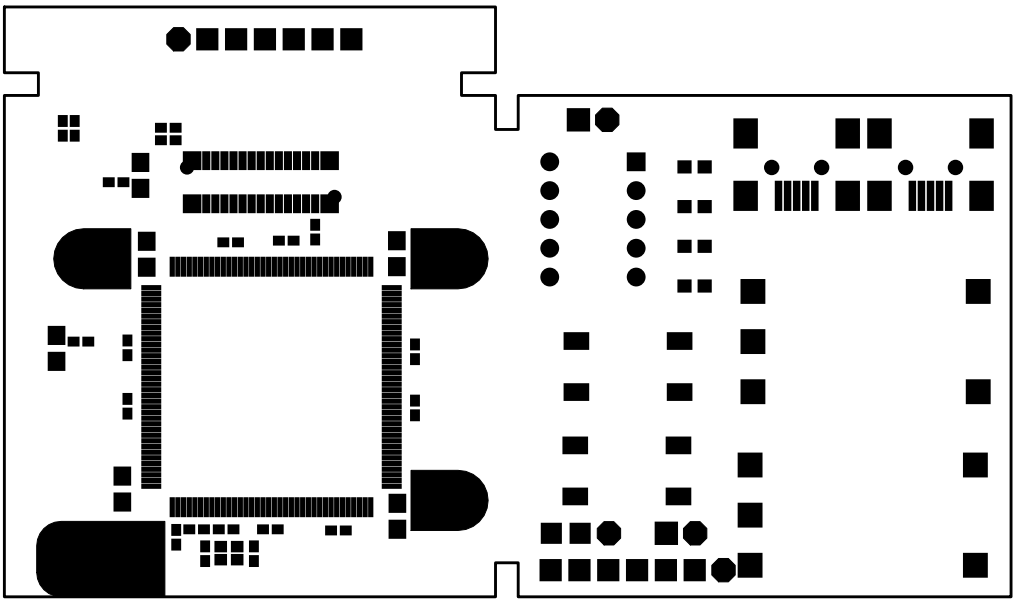

Figure 43. Bottom mask (scale 1.5).

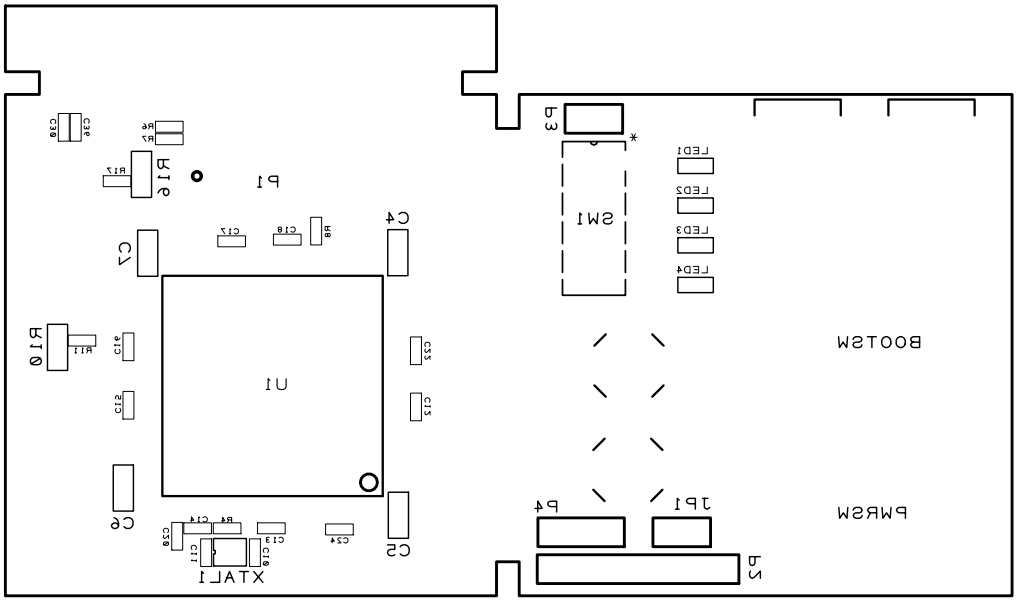

Figure 44. Bottom silkscreen (scale 1.5).

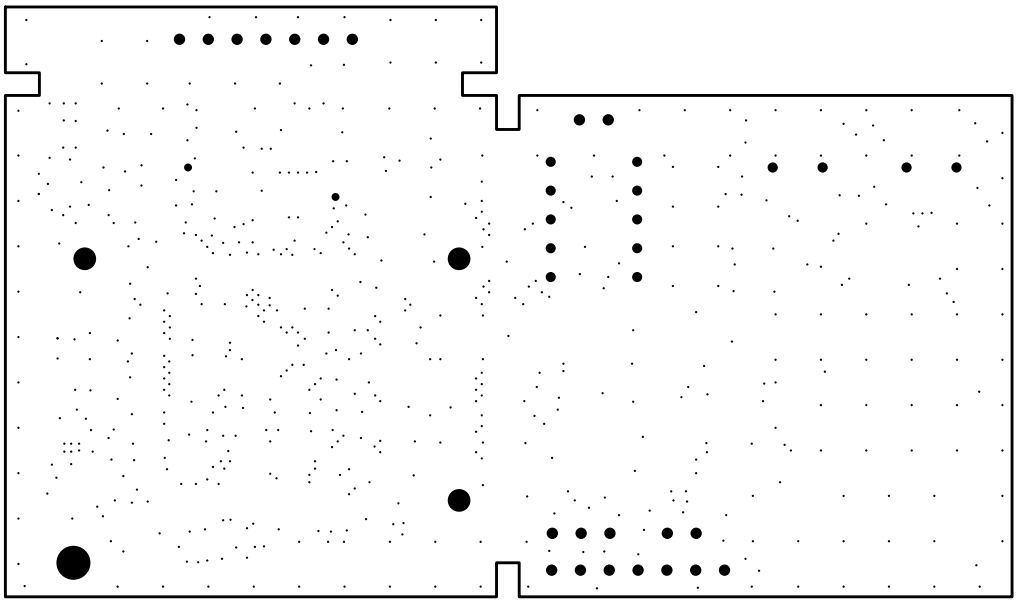

Figure 45. Drill data (scale 1.5).

Appendix F Sensor PCB layout

Figure 46. Board outline (scale 1.5).

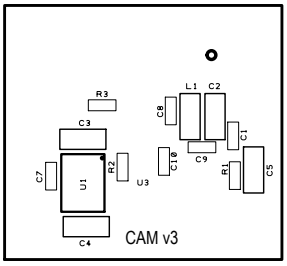

Figure 47. Top silkscreen (scale 1.5).

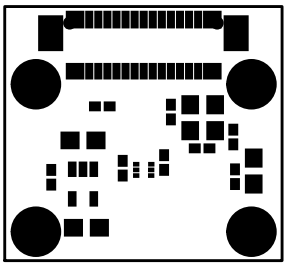

Figure 48. Top mask (scale 1.5).

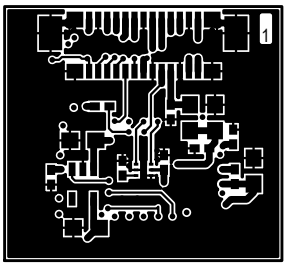

Figure 49. Top copper (scale 1.5).

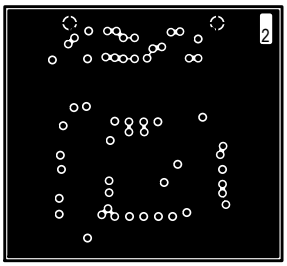

Figure 50. Inner 1 - ground(scale 1.5).

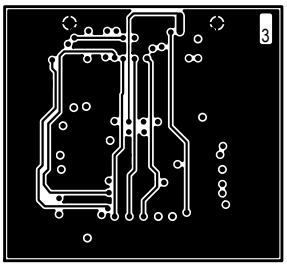

Figure 51. Inner 2 (scale 1.5).

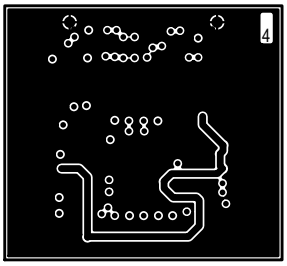

Figure 52. Inner 3 - power (scale 1.5).

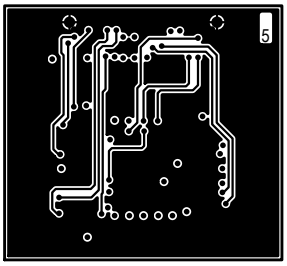

Figure 53. Inner 4 (scale 1.5).

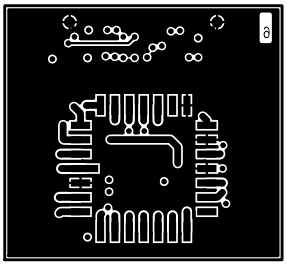

Figure 54. Bottom copper (scale 1.5).

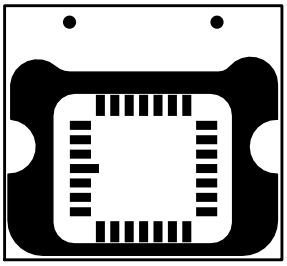

Figure 55. Bottom mask (scale 1.5).

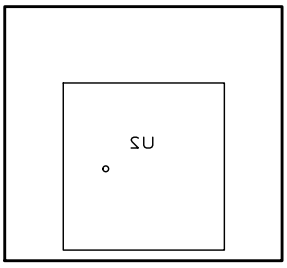

Figure 56. Bottom silkscreen (scale 1.5).

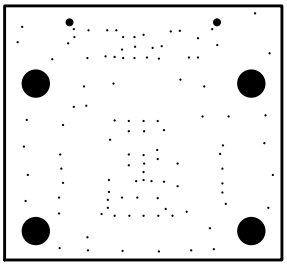

Figure 57. Drill data (scale 1.5).

Appendix G CD contents

Table 6. Contents of the accompanying CD.

Final design	Final design schematics and layout in DesignSpark and Gerber formats
Firmware	Second prototype firmware
Prototype v2	Second prototype schematics and layout
PyCAM	PyCAM testing software
Test results	Testing result data
B2012_Kuuste.pdf	A copy of the thesis
EC1 CAM phase-B.pdf	ESTCube-1 camera phase B report
EC1 CDHS phase-A.pdf	ESTCube-1 CDHS phase A report
EC1 ENVI phase-B.docx	ESTCube-1 ENVI phase B report
readme.txt	Detailed description of CD contents